Development of integrated approach employing Fe/TiO$_2$-[BMIM]FeCl$_4$ system for sulfur removal from model oil

By

Den Agustino Bin Fakhrol

9076

Dissertation submitted in partial fulfillment of

the requirements for the

Bachelor of Engineering (Hons)

(Chemical Engineering)

NOVEMBER 2010

Universiti Teknologi PETRONAS

Bandar Seri Iskandar

31750 Tronoh

Perak Darul Ridzuan

TABLE OF CONTENT

LIST OF FIGURES

LIST OF TABLES

CERTIFICATION OF APPROVAL

Development of integrated approach employing Fe/TiO$_2$-[BMIM]FeCl$_4$ system for sulfur removal from model oil

By

Den Agustino B Fakhrol

A project dissertation submitted to the

Chemical Engineering Programme

Universiti Teknologi PETRONAS

In partial fulfillment of the requirement for the

BACHELOR OF ENGINEERING (Hons)

(CHEMICAL ENGINEERING)

Approved by,

_____

(AP. Dr Chong Fai Kait)

UNIVERSITI TEKNOLOGI PETRONAS

TRONOH, PERAK

JULY 2010

CERTIFICATION OF ORIGINALITY

This is to certify that I am responsible for the work submitted in this project, that the original work is my own except as specified in the references and acknowledgements, and that the original work contained herein have not been undertaken or done by unspecified sources or persons.

_____

(DEN AGUSTINO BIN FAKHROL)

ABSTRACT

This project researchs on the development of TiO_2 semiconductors doped with Iron, Fe as the photocatalyst and ionic liquid, [BMIM]$FeCl_4$ for desulfurization process of model oil. Current technology for desulfurization requires severe process conditions; high pressure and temperature in order to remove the sulfur compounds in crude oil. Therefore, research is being conducted to develop better desulfurization process employing photocatalysis and liquid-liquid extraction conducted at atmospheric pressure and temperature in the presence oxygen. TiO_2 was selected as the photocatalyst but not active in visible light. So, modification was done by doping the TiO_2 photocatalyst with transition metals, Iron, Fe. Transition metal doping is able to enhance the photoexcitation of electrons in the photocatalyst when only subjected to visible light. Besides, it can act as charge carrier trapper for both photogenerated electrons and holes thus inhibiting the electron-holes recombination for longer time. Wet Impregnation method was chosen to prepare iron-doped catalyst, using Iron(III) Nitrate, $Fe(NO_3)_3$ as starting materials. The dopant loading varied from 0.4 to 0.8wt% and two calcination temperatures were selected which are 400°C and 500°C. Characterization of the modified photocatalysts were done by X-Ray Diffraction (XRD), UV-vis Diffuse Reflectance Spectra (UV-vis DRS), Field Emission Scanning Electron Microscopy (FE-SEM) and Fourier Transform Infrared Spectroscopy (FTIR). In this project, 1-butyl-3-methylimidazolium tetrachloroferrate , [BMIM]$FeCl_4$ was preferred as the ionic liquid for liquid-liquid extraction process as it involved same element with the transition metal doped to TiO_2. [BMIM]$FeCl_4$ was prepared by mixing together anhydrous Iron(III) Chloride, $FeCl_3$ and 1-butyl-3-methylimidazolium chloride, [BMIM]Cl. The desulfurization analysis using halogen lamp and Gas Chromatography, GC analysis was done to investigate the photocatalytic activity of the modified photocatalysts and extraction process by ionic liquid. It was found that 0.6wt% of Fe/TiO_2 calcined at 400°C yield, thus chosen for the integrated approach combining with ionic liquid, [BMIM]$FeCl_4$. The integrated approach also showed the increment of sulfur removal from using photocatalyst and model oil alone. The reduction of band gap as a result of doping was estimated and the influence of the process parameters on catalytic activity is explained.

ACKNOWLEDGEMENT

CHAPTER 1

INTRODUCTION

1.1　Background of Study

Liquid fuels contain a large variety of sulfur compound (thiols, sulfides, disulfides and thiophenes), which generate sulfur dioxide, SO_2 and airborne particulate emissions during combustion, and hydrogen sulfide, H_2S during refinery process (Campos M. J. M., *et al.* (2010), Takayuki H., *et al.* (1996)). The emission of SO_2 and H_2S is one of the main contributors to acid rain and water pollution (Takayuki H., *et al.* (1996)). Concerning the issue, rules and regulations regarding these emissions to environment were made to ensure that refineries adhere to efforts of the government to reduce the sulfur content in fuel product.

At current time, the most important and common industrial process is that of treating the fuel under high temperatures and high pressures with hydrogen (Campos M. J. M., *et al.* (2010)). This process is called catalytic hydrodesulfurization (HDS) and has received extensive attention since its discovery in 1930's (Campos M. J. M., *et al.* (2010)). HDS is commonly used for sulfur removal from fuels. This process involves high temperatures exceeding 300 °C, elevated pressures of over 2 MPa, precious metal catalysts, high hydrogen consumption, and large reactors (Hiroaki T., *et al.* (2009)). The refractory sulfur, dibenzothiophenes (DBTs), especially 4 and/or 6 alkyl-substituted DBTs are difficult to remove using the HDS process unless an energy-intensive process is applied (Hiroaki T., *et al.* (2009)).

Research regarding the development of better technology for desulfurization, which reduce the energy consumption and other than HDS is conducted. Processes such as

extraction, alkylation, oxidation an adsorption are considered, and among these process, oxidative desulfurization is seen most potential solution as it can be applied in mild condition, at ambient pressure and temperature (Campos M. J. M., *et al.* (2010), Hiroaki T., *et al.* (2009)).

Oxidative desulfurization process including microbial oxidation, chemical oxidation and photooxidation generally lead to the formation of sulfoxides or sulfones that can be subsequently removed by conventional separation methods such as extraction, adsorption or distillation (Hiroaki T., *et al.* (2009)). Interests have been focused on photooxidation because of the possibility of using atmospheric oxygen as an oxidizing agent (Hiroaki T., *et al.* (2009)).

1.2   Problem Statement

In term of the current issues, the sulfur presence in crude oil in the main contributor to the formation of SO_2 and H_2S that can bring harms to living organism, environment and process plant itself. High sulfur content in crude oil can negatively affect the refinery performance, as it can act as poison to reforming photocatalyst. Besides, sulfur content can cause corrosion to the equipments and pipelines. Environmentally, emissions of SO_2 and H_2S can promote the formation of acid rain and causing air pollution. Besides, H_2S can cause irritation to conjunctiva, skin and mucous membrane as well as reacting with enzymes in bloodstreams and inhibit cellular respiration resulting in pulmonary paralysis; sudden collapse and death (refer H_2S MSDS).

In term of photocatalyst used, TiO_2 which will be later discussed and explained in the next chapter, is not active in visible light, only active in UV-light region (UV-active) and the feasibility of the photocatalyst for desulfurization process is not proven yet. Modification by transition metal doping, which is Iron, Fe will be done to extend the activation of the photocatalyst from only UV region to visible light region. By doing so, the desulfurization process can utilize the abundant energy from sunlight.

1.3 Objective

The objectives of this project are:

- To develop the Fe-TiO$_2$ photocatalyst to be feasible and effective for process of sulfur removal from model oil
- To combine photocatalysis (Fe/TiO2) and extraction (ionic liquid) into an integrated system for sulfur removal from model oil

1.4 Scope of Study

This project is researching on the utilization of photocatalyst, semiconductor as the oxidizing agent of the sulfur compound in model oil via photocatalytic oxidation. Interest regarding the photocatalytic oxidation process is focused due to the condition of the process which is in moderate condition, plus the presence of light. The photocatalyst will be prepared in laboratory, and then the synthesized photocatalyst will be characterized using methods such as X-ray Diffraction, Field Emission Scanning Electron Microscopy (FE-SEM) and others to determine the physical properties. After completing the characterization, test regarding the feasibility and effectiveness of the synthesized photocatalyst will be conducted using sulfur species dissolved in model oil. The photocatalytic desulfurization is analyzed, monitored time by time and recorded accurately. Then, the result of the experiment will be analyzed to determine the feasibility of photocatalyst in desulfurization process.

CHAPTER 2
LITERATURE REVIEW

2.1   Photocatalyst

Photocatalyst produces surface oxidation to eliminate harmful substances such as organic compounds or nearby bacteria, when it is exposed to the sun or fluorescent lamp. TiO_2 is a semiconductor which turns to a high-energy state by receiving light energy, and releases electrons from its illuminated surface. If the energy received at this stage is high enough, electrons that were initially located in the so-called 'valence band' all jump up to the 'conduction band'.

Fujishima and Honda discovered the photocatalytic splitting of water on TiO_2 e1ectrodes in 1972, marking the new beginning for research for heterogeneous photocatalysis (Amy L. L., *et al.*(1995)). Researches have been conducted on the photocatalyst for the purpose of understanding the fundamental photo-electrochemistry process, its feasibility and to improve the photocatalytic efficiency of the semiconductor. Semiconducting metal oxides such as TiO_2, $SrTiO_3$, Fe_2O_3, and Pt were much used for these researches; however TiO_2 is the most preferable (Aboel M. A., *et al.* (1998)). The strong oxidizing power of the photogenerated holes (large band gap material), the chemical inertness and resistance to both photocorrosion and decomposition reactions which plague other band gap materials (e.g., Si, GaAs, GaP, lnP, CdS, etc.), low cost and wide availability in addition to the nontoxicity of TiO2 have made it a superior photocatalyst (Aboel M. A., *et al.* (1998)).

2.2 Titanium (IV) Oxide, TiO₂ as Photocatalyst

Unlike metals which have a continuum of electronic states, semiconductors possess a void energy region where no energy levels are available to promote recombination of an electron and hole produced by photoactivation in the solid. The void region which extends from the top of the filled valence band to the bottom of the vacant conduction band is called the band gap. Once excitation occurs across the band gap there is a sufficient lifetime, in the nanosecond regime, for the created electron-hole pair to undergo charge transfer to adsorbed species on the semiconductor surface from solution or gas phase contact. If the semiconductor remains intact and the charge transfer to the adsorbed species is continuous and exothermic the process is termed heterogeneous photocatalysis (Amy L. L., *et al.* (1995)).

The initial process for heterogeneous photocatalysis of organic and inorganic compounds by semiconductors is the generation of electron-hole pairs in the semiconductor particles. The enlarged section of Figure 1 shows the excitation of an electron from the valence band to the conduction band initiated by light absorption with energy equal to or greater than the band gap of the semiconductor. Upon excitation, the fate of the separated electron and hole can follow several pathways. Figure 2.1 illustrates some of the deexcitation pathways for the electrons and holes (Amy L. L., *et al.*(1995)).
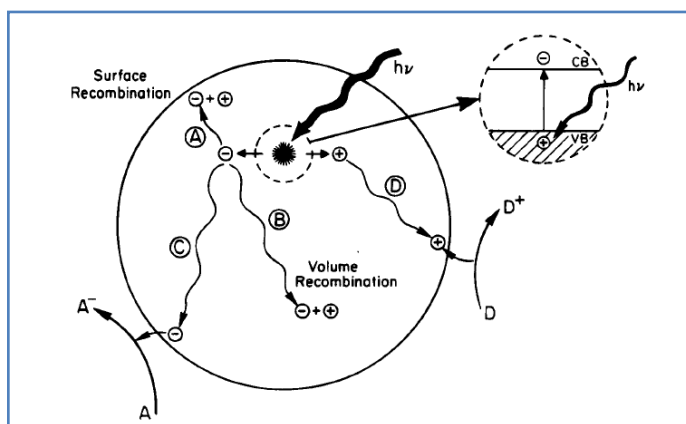
FIGURE 2.1: Schematic photoexcitation in a solid followed by deexcitation events

The photoinduced electron transfer to adsorbed organic or inorganic species or to the solvent results from migration of electrons and holes to the semiconductor surface. The electron transfer process is more efficient if the species are preadsorbed on the surface. While at the surface the semiconductor can donate electrons to reduce an electron acceptor (usually oxygen in an aerated solution) (pathway **C);** in turn, a hole can migrate to the surface where an electron from a donor species can combine with the surface hole oxidizing the donor species (pathway D)

TiO_2 has been widely studied because of its various merits, such as optical-electronic properties, low-cost, chemical stability, and non-toxicity (Tianzhong T., *et al.* (2008)). However, it is unavoidable to face two issues for its practical applications, one of which is to improve the low photo-quantum efficiency of TiO_2 that arises from the fast recombination of photogenerated electrons and holes; another is to further extend its photoresponse into visible light regions (Tianzhong T., *et al.* (2008)). Particularly, TiO_2 can only be activated by UV light due to its large band gap (Ebg, anatase≈3.2 eV, Ebg, rutile≈3.0 eV) and only make use of 3–5% of the solar spectrum that reach the earth (Tianzhong T., *et al.* (2008)).

One of solutions to enhance the performance of TiO_2 photocatalyst is by doping the photocatalyst with suitable transition metal, which is in this project, Iron, Fe is selected.

2.3 Transition Metal Doping of TiO$_2$ photocatalyst

2.3.1 Charge Carrier Trapping

Due to the low photo-quantum efficiency of TiO$_2$, recombination of the photoexcited electron-hole pair needs to be retarded for an efficient charge transfer process to occur on the photocatalyst surface. Charge carrier trapping would suppress recombination and increase the lifetime of the separated electron and hole to above a fraction of a nanosecond (Amy L. L., *et al.*(1995))..

A simplified illustration of available bulk and surface trapping states for a photogenerated electron in a semiconductor is shown in Figure 2.2. In this illustration, the energy levels of the bulk and surface state traps fall within the band gap of the semiconductor. These surface and bulk states are localized. The charge carriers trapped in such states are localized to a particular site on the surface or in the bulk. The population of bulk and surface traps is dependent on the energy difference between the trap and the bottom of the conduction band and the decrease in entropy when the electron undergoes trapping (Amy L. L., *et al.*(1995))..
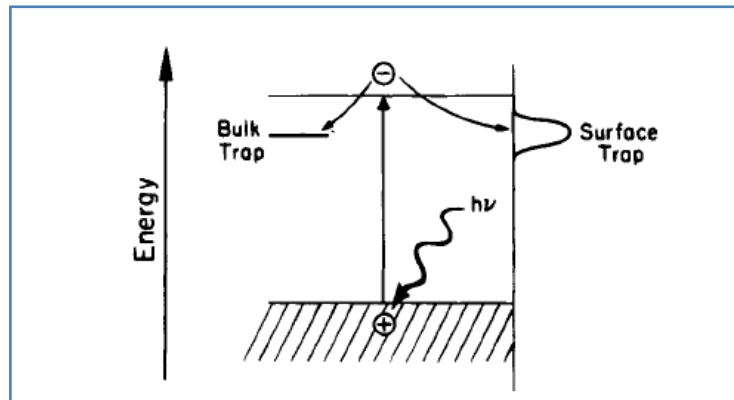
FIGURE 2.2: Surface and bulk electron carrier trapping

The example for charge carrier trapping can be observed from a photocatalytic study of Ce-TiO$_2$ photocatalyst (Tianzhong T., *et al.* (2007)). Ce^{4+} ion acts as an electron scavenger to trap the electron of excited dye molecule. The electron trapped in Ce^{4+} sites was subsequently transferred to adsorption O$_2$ to form oxygen radicals. The release of the oxygen radical will further initiate the photocatalytic reaction (Tianzhong T., *et al.* (2007)).

2.3.2   Fe^{3+} Doped to TiO$_2$ Photocatalyst

It is necessary to develop a proficient way to not only extend the absorbance of TiO2 into visible regions but also reduce the recombination of photo-generated electrons and photogenerated holes. Recently, some studies have reported doping with suitable transitional metals is a useful way for improving the above two performances of TiO$_2$, and amongst variety of transitional metals, iron has been considered to be an appropriate candidate due to the fact that the radium of Fe^{3+} (0.69 A) is similar to that of Ti^{4+} (0.745 A), so Fe^{3+} can be easily incorporated into the crystal lattice of TiO$_2$ (Tianzhong T., *et al.* (2008)).

The most accepted explanation for the improved photocatalytic performance of iron-doped photocatalyst is the generation of shallow charge traps in the crystal structure which decreases the recombination rate of electron–hole pairs. At the same time, the absorption of light is improved. Introducing iron ions into the lattice therefore provides photocatalysts not only with lower electron–hole recombination rate but also with excitability by visible light. Enhanced photocatalytic activity was observed for iron-doped photocatalyst under UV and also for visible light irradiation in several publications both in gas and in liquid phase, for a variety of model compounds (e.g., dye molecules, phenols, oxalic acid, acetaldehyde, acetone, 2- propanol, etc.) (Zolta´n A., *et al.* (2008)).

It can be found that Fe doping almost has no influences on the crystal structure and morphology of the photocatalyst. Although Fe doping affects the crystal size and specific surface area (S_{BET}) of the photocatalyst to a certain extent, the photocatalytic activity of the catalysts is not in accordance with the variations of crystal size and S_{BET}. The effect of Fe^{3+} doping on the photocatalytic activity under UV light irradiation should be due to the reason that an appropriate amount of Fe^{3+} ions can act as intermediates for photo-generated holes and electrons transfer, and inhibit the recombination of holes and electrons. Due to the facts that the energy level for Fe^{3+}/Fe^{4+} is above the valence band edge of TiO_2 and the energy level for Fe^{3+}/Fe^{2+} is below the conduction band edge of TiO2, Fe^{3+} ions, acting as both electrons and holes traps, can turn into Fe^{2+} and Fe^{4+} ions by trapping photo-generated electrons and holes traps, respectively.

According to the viewpoint of crystal field theory, Fe^{2+} and Fe^{4+} ions are relatively unstable when compared to Fe^{3+} ions, which have half-filled 3d5 orbital. Therefore, the trapped charges can easily release from Fe^{2+} or Fe^{4+} ions and then migrate to the surface to initiate the photocatalytic reaction. Fe^{2+} ions can be oxidized to Fe^{3+} ions by transferring electrons to absorbed O_2 on the surface of TiO_2 or neighboring surface Ti^{4+} ions. Meanwhile, the adsorbed O_2 is reduced to O^{2-}, which can further degrade MO (see figure 2.3). Similarly, Fe^{4+} ions also are reduced to Fe^{3+} ions by releasing electrons, while surface hydroxyl group translates into hydroxyl radical. As a result, the introduction of appropriate Fe^{3+} ions is responsible for the reduction of the photo-generated hole–electron recombination rate and favors the improvement of the photocatalytic activity (Tianzhong T., *et al.* (2008)).
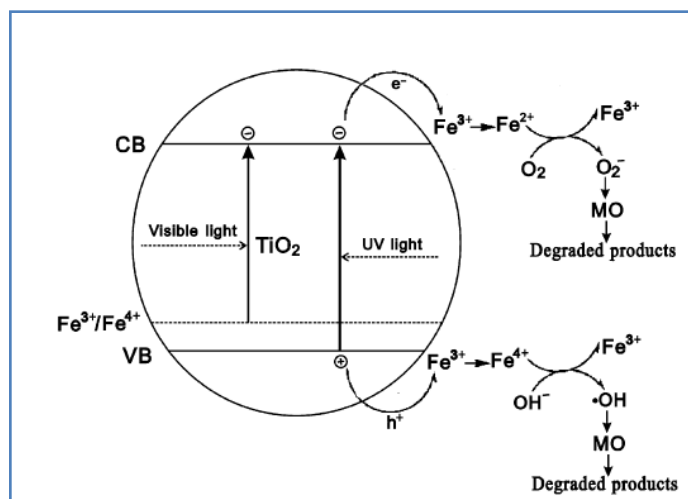
FIGURE 2.3: Proposed mechanism for MO degradation under UV and visible light irradiation

However, when the concentration of Fe^{3+} ions becomes too large, Fe^{3+} ions can act as the recombination centers for the photo-generated electrons and holes, resulting in the decrease of photocatalytic activity (Tianzhong T., *et al.* (2008)). So, optimal concentration of Fe^{3+} is needed for maximum photocatalytic activity.

2.4   Ionic Liquid

Over the past years the desulfurization of various motor fuels has been suggested to be performed by extraction with ionic liquids (Campos M. J. M., *et al.* (2010), Anisimov A, *et al.* (2009)). They are sometimes referred to as non-aqueous ionic liquids (NAILs) or molten salts (Paul J. D., (2002)) . Ionic liquids are a new class of solvents which have interesting properties such as non-volatility, high ionic concentration, good thermal stability, non-flammability and can dissolve most of organic as well as inorganic materials (Shadpour M., *et al.* (2006)). Ionic liquids containing Cu (I) and Ag (I) ions were found to be especially efficient due to their tendency to form π complexes with thiophene derivatives (Campos M. J. M., *et al.* (2010), Chongpin H., *et al.* (2004)).

An interesting example is the application of ionic liquids obtained by reaction of 1-butyl-3-methylimidazolium chloride [BMIM]Cl with anhydrous powdered CuCl, containing $CuCl_2^-$, $Cu_2Cl_3^-$, and $Cu_3Cl_4^-$ anions that are resistant to moisture and air, for desulfurization of a model fuel. These systems revealed a high desulfurizing activity toward gasoline; for instance, the ionic liquid $BMImCu_2Cl_3$ extracted 23% of sulfur compounds, whereas $BMImBF_4$ extracted no more than 11%. Potent complex-forming agents dissolved in gasoline hinder extraction of sulfur compounds with ionic liquids (Campos M. J. M., *et al.* (2010)). As for the project, $[BMIM]FeCl_4$ is used as it uses same element of the doping metal, Iron, Fe. Besides, $[BMIM]Cu_2Cl_3$ is also prepared. This liquid has been called an ionic liquid and has been receiving increased attention in separation processes for its non-volatility (Chongpin H., *et al.* (2004)).

Ionic liquids can be regenerated by treatment of the extract with an excess of low-boiling paraffins and repeatedly used for desulfurization. But, as a general rule, ionic liquids themselves, in the absence of oxidants, fail to provide a high degree of sulfur removal. This effect can be related to the similar polarity between alkenes, aromatics, and the sulfur compounds, and the sulfur removal is improved increasing the polarity of sulfur oxidizing sulfur compounds to the corresponding sulfoxides and sulfones (Campos M. J. M., *et al.* (2010)).

2.5 Photooxidation Mechanism of Selected Sulfur Compound

The photocatalytic oxidation of dibenzothiphene (selected sulfur species) gives mainly corresponding sulfoxide and sulfone from mechanism shown below (Aboel M. A., *et al.* (1998)):
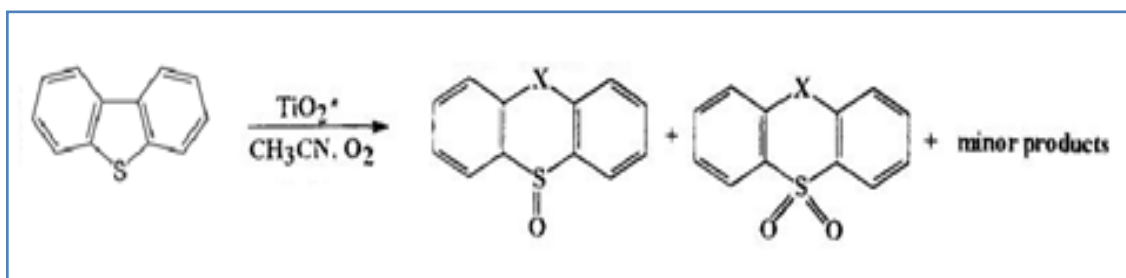
FIGURE 2.4: Reaction Chemistry of Photooxidation of Dibenzothiophene

For other sulfur species (I: dibenzothiphene, II: thioxanthone, and III: thianthrene):
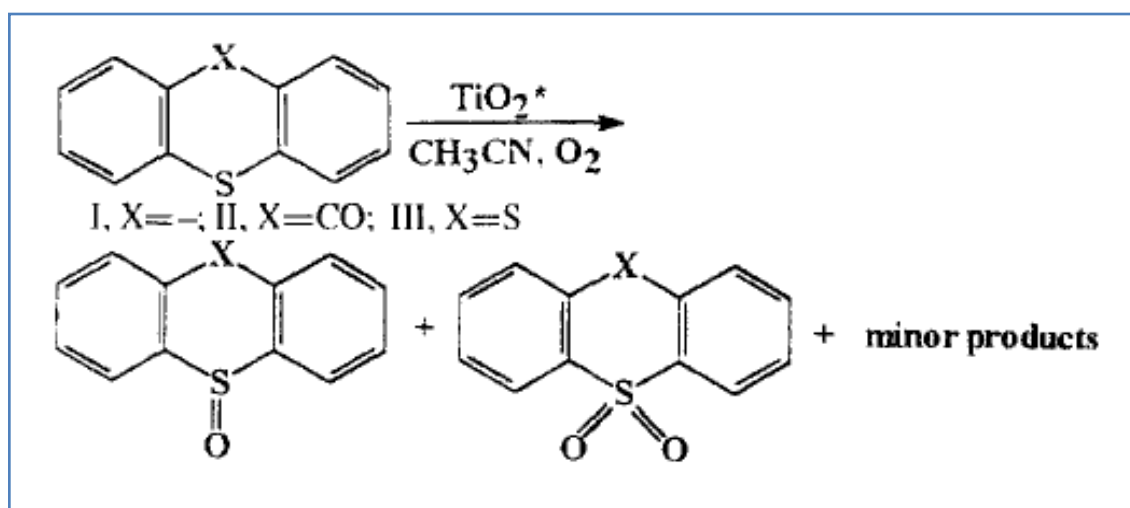
FIGURE 2.5: General sulfur Photooxidation Route

2.6   Integrated System of Photooxidation - Ionic Liquid Extraction Approach for Sulfur Removal

Integrated approach employing both photooxidation and extraction using ionic liquid has yet been explored by researches. In this project, the best modified photocatalyst judge by the sulfur removal percentage with the given condition will be used together with ionic liquid, maintaining their original ratio to the model oil, for the observation of integrated approach of photooxidation and extraction of sulfur compound in model oil. There are two possible mechanisms for integrated approach for desulfurization using photooxidation-extraction which are photooxidation in ionic liquid phase and photooxidation in model oil phase.

2.6.1   Mechanism 1: Photooxidation in Ionic Liquid Phase

In this mechanism, sulfur compounds were initially extracted in large quantities from model oil phase into ionic liquid phase. Photodegradation of Fe^{3+} would create radical (O_2^- and ^-OH) and since the ionic liquid consisted of anion and cation and has a lower dielectric, it may be excellent medium for existence of radical ions (Dishun Z., (2008)). The radical ions transfer into the ionic liquid phase easily and exist stably which leads to a high concentration of oxidizing agent (O_2^- and ^-OH radical). The sulfur compounds dissolved in the ionic liquid phase are then oxidized by the oxidizing agent since the oxide products DBTO and $DBTO_2$ have higher solubility in the ionic liquid. So once the previously extracted sulfur compounds were oxidized in ionic liquid phase, the remaining sulfur compounds in the model oil phase can be successfully extracted from the model oil to the ionic liquid phase and oxidized. In the end, the continuous decrease in concentration of sulfur compounds in model oil is observed during process can be attributes to the large numbers of sulfur compounds that can be oxidized in the ionic liquid phase by the oxidizing agent accordingly.

2.6.2 Mechanism 2: Photooxidation in Model Oil Phase

Modified photocatalyst subjected to visible light irradiation will induce the photodegradation of Fe^{3+} in which creating radicals (O_2^- and ^-OH). The radicals in turn oxidize the sulfur compounds in the model oil phase to form highly polarized compounds, sulfones and sulfoxides. These two do not distribute into the nonpolar model oil and much easier to be extracted into the ionic liquid phase in which is a polar compound. So, the extraction of sulfur compounds happen simultaneously with the extraction of the oxidized sulfur compounds. The decrease in concentration of sulfur compounds in model oil is caused by the oxidation of the sulfur compounds in the model oil phase and its extraction into ionic liquid phase by attraction of polar compounds.

CHAPTER 3

METHODOLOGY

```
┌─────────────────┐     ┌─────────────────┐     ┌─────────────────┐
│    Fe/TiO₂      │     │                 │     │  Ionic Liquid   │
│  photocatalyst  │     │    Model oil    │     │  [BMIM]FeCl₄    │
│   preparation   │     │   preparation   │     │   preparation   │
└─────────────────┘     └─────────────────┘     └─────────────────┘

┌─────────────────┐                             ┌─────────────────┐
│    Fe/TiO₂      │                             │  Ionic liquid   │
│ characterization│                             │ characterization│
└─────────────────┘                             └─────────────────┘

        ┌──────────────────────────────────────────────────┐
        │  Desulfurization process using Fe/TiO₂ photocatalyst │
        │        with and without [BMIM]FeCl₄              │
        └──────────────────────────────────────────────────┘
```
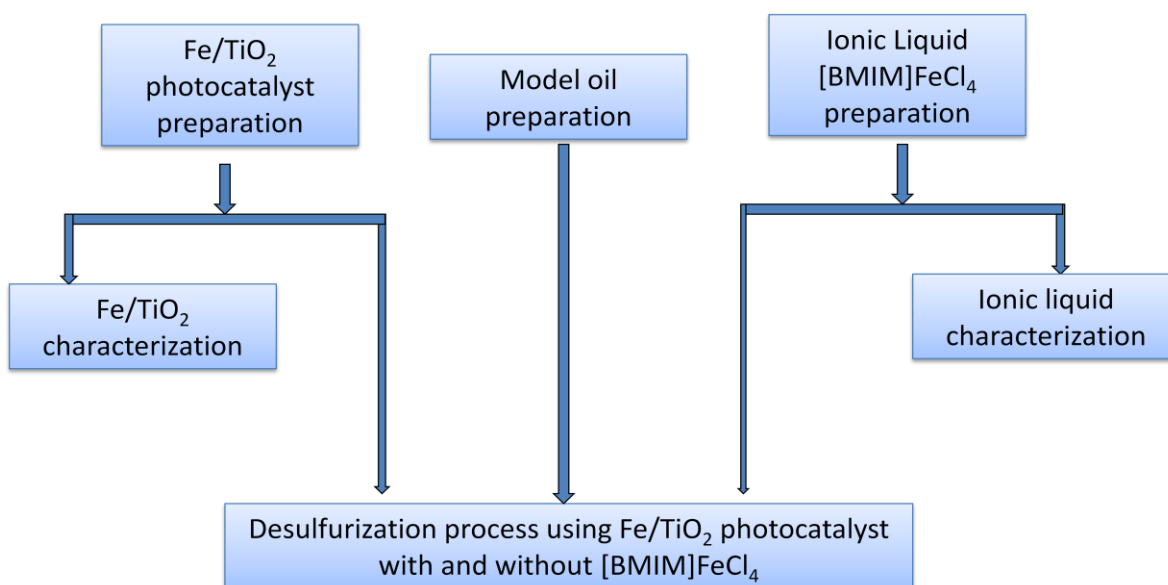
FIGURE 3.1: Overview on the methodology of experiment

3.1 Iron-Titania, Fe/TiO₂ photocatalyst

The selection of photocatalyst (TiO_2 and modified TiO_2) and its preparations are obtained from literature review. For this project, the photocatalysts used are pure TiO_2 and Fe^{3+} doped TiO_2. The preparation methods are as below:

3.1.1 Preparation and Pretreatment of Fe^{3+}-TiO_2 photocatalyst

The preparation method for Fe^{3+}-TiO_2 photocatalyst is very important to determine the improvement of the photocatalytic activity. The effect of the transition metal doping and the concentration of doped Fe will affect the photocatalytic activity of the modified photocatalyst (Tianzhong T., *et al.* (2007)). Fe^{3+}-TiO_2 photocatalyst can be prepared by several techniques such as hydrothermal treatment (Tianzhong T., *et al.* (2008)), wet impregnation (Zolta´n A., *et al.* (2008)), sol-gel technique (Jiefang Z., *et al.* (2006)), ultrasonic (Zhou M, *et al.* (2006)) and co-precipitation (Tianzhong T., *et al.* (2007)).

For this project, Fe^{3+}-TiO_2 photocatalyst will be prepared using wet impregnation method due to its simplicity and extremely versatile techniques which can be controlled to give a good dispersion and better distribution of metal loading on the support.

The percentage of Iron, Fe doped into TiO_2 is 0.4 wt%, 0.6 wt% and 0.8wt%. A calculated amount of copper nitrate in distilled water being stirred for 1 hour with TiO_2 added to it. (Calculation in Appendix A) The solvent has been evaporated slowly in water bath at $80^{\circ}C$ until the solvent has transform into super-saturated solvent. The solvent being oven-dried at $120^{\circ}C$ for 18 hours. The dried solution being grinded to get the photocatalyst in powder form. This is to ensure that the photocatalyst get the maximum surface area contact during calcinations. Finally, calcination process which is to remove NO_3^- substance been conducted at 400°C and 500°C for 1 hour. Figure 3.2 is the summary of the preparation of Fe/TiO_2 methodology.
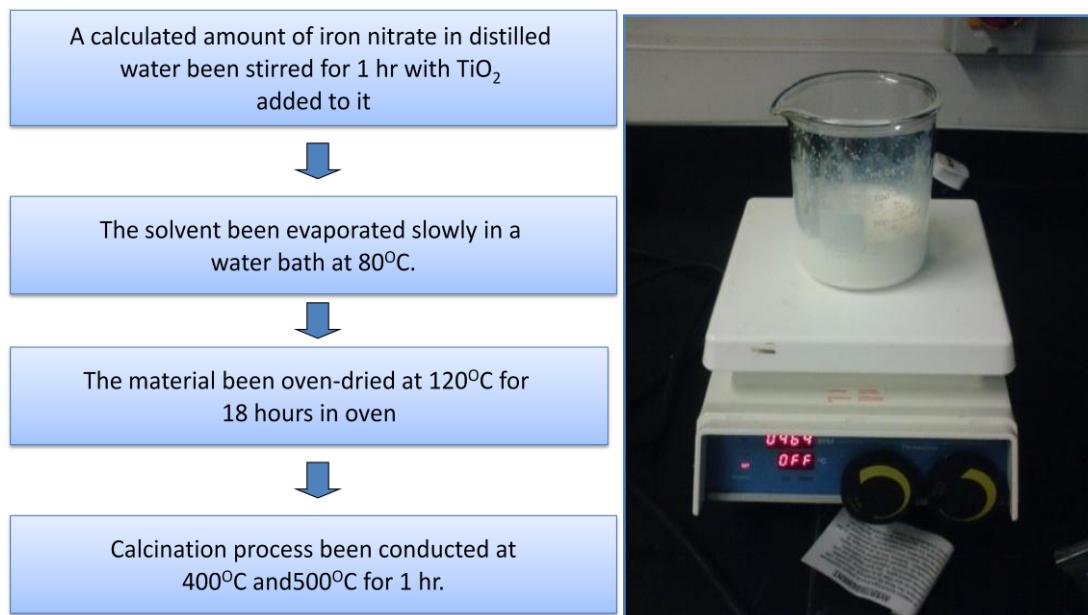
FIGURE 3.2: Flowchart for Fe^{3+}-TiO_2 photocatalyst preparation (left) and picture of $Fe(NO_3)_3$ mixed with TiO_2(right)

The amount of Fe metal loading to TiO_2 are based on target of having Fe concentration of 0.4, 0.6 and 0.8wt% of Fe in TiO_2. This variation of concentrations was done to observe the dependence of the photocatalysts' performance to the amount of dopant. This concentration is decided based on literature review and continuations of previous project that showing decrement of photocatalytic activity between concentrations of 0.4 to 1.0wt% of Fe in TiO_2. The experiment also been carried out in three different calcinations temperature which are 400°C and 500°C. This is to determine the suitable calcinations temperature for the photocatalyst. This calcinations temperature is taken based on literature review. Calcination can activate the catalyst and also reduce the concentration of nitrate from Iron(III) Nitrate in photocatalyst .

The details of the photocatalysts prepared:

Metal loading (wt %)	Calcinations temperature (°C)	
	400	500
0.4	0.4FeTiO400	0.4FeTiO500
0.6	0.6FeTiO400	0.6FeTiO500
0.8	0.8FeTiO400	0.8FeTiO500

TABLE 3.1: Details of the photocatalysts prepared

The prepared photocatalyst will then undergo the characterization process before being used for photocatalytic desulfurization experiment. This process is to ensure that Fe^{3+} ion is successfully doped into TiO_2 photocatalyst surface.

3.1.2   Characterization of the Photocatalyst

Characterization of the photocatalyst is essential procedure to determine the physical properties of the photocatalyst. The characterization methods used are as below:

3.1.2.1 X-Ray Diffraction (XRD)

This test is done to determine the phases, crystal structures and crystallite sizes of the modified TiO_2 photocatalyst. It is performed on an X-Ray Diffractometer at room temperature. The crystallite size observed in XRD can be calculated using the Scherrer's equation (Tianzhong T., *et al.* (2008)).

3.1.2.2 UV-vis Diffuse Reflectance Spectra (DRS)

This test is conducted using UV-vis-NIR spectrophotometer to determine the optical properties of the modified TiO_2 photocatalyst. Optical properties refer to the light region adsorption ability of the photocatalyst. Using this analysis, it would show the absorbance of light has been shifted to the visible region after TiO_2 is doped with Fe metal. The diffuse reflectance UV-vis spectra of the photocatalysts are recorded by the equipment with an integrating sphere attachment using $BaSO_4$ powder as reference. The photocatalyst samples are prepared in sample holder, thick enough so that all incident light to be absorbed or scattered before reaching the back surface of the sample holder. Resulting diffuse reflectance spectra are plotted as the Kubelka-Munk fuction or remission, F(R) versus wavelength. The band gap energy (E_g) for all photocatalysts are determined from the extrapolation of the linear fit for the Tauc plot onto the photon energy axis as the relationship below depicts:

$$[F(R).hv]^{1/2} \quad = K(hv - E_g)$$

Where hv is photon energy and K is the constant characteristic of the semiconductor material.

3.1.2.3 Field Emission Scanning Electron Microscopy (FE-SEM)

This test is conducted to show how well the dopant is dispersed into TiO_2. From the morphologies obtained from the photocatalysts, determinations of the distribution of Fe inside TiO_2 structure are done. Besides, from Energy Dispersive X-Ray (EDX) analysis, elemental analyses are done to determine Fe element in photocatalysts prepared. Using FE-SEM, the samples are coated with a layer of platinum-palladium before scanning at 100K magnification.

FIGURE 3.3: Picture of Field Emission Scanning Electron Microscopy (FE-SEM)

3.1.2.4 Fourier Transform Infrared Spectroscopy (FTIR)

This test is for identifying chemicals that are either organic or inorganic. It can be utilized to quantitate some components of an unknown mixture. FTIR spectra are useful to determine the functional group (NO_3^-, OH^- and etc) present in photocatalysts before and after the calcinations process. They are identified by characteristic peaks in the spectrum. Using FTIR, a sample is prepared by grinding and mixing approximately 1mg of photocatalyst and 200mg of IR-grade KBr and the samples are pressed into a pellet by hand press. The FTIR spectrum of the pellet, taken over a wavelength range of $450 cm^{-1}$ to $4000 cm^{-1}$, recorded as the percentage of transmittance (%T) versus wavelength.

FIGURE 3.4: Picture of Fourier Transform Infrared spectrophotometer.

3.2 Ionic Liquid: 1-butyl-3-methylimidazolium tetrachloroferrate, [BMIM]FeCl$_4$

3.2.1 [BMIM]FeCl$_4$ Preparation Using Anhydrous Iron(III) Chloride, FeCl$_3$

In preparing 1-butyl-3-methylimidazolium tetrachloroferrate, [BMIM]FeCl$_4$, a method using anhydrous FeCl$_3$ is adopted from literature review.

In a round bottom flask equipped with a magnetic stirrer, calculated amount anhydrous FeCl$_3$ were slowly added to calculated amount 1-butyl-3-methylimidazolium chloride, [BMIM]Cl. To ensure complete reaction, the reaction mixture was left stirring overnight (Calculation of the amount of materials needed available in Appendix B). A red-brown liquid was obtained which was dried under high vacuum and stored under N$_2$. (Iraj M. B., *et al*, (2010))

3.3   Desulfurization of Model Oil Analysis

3.3.1   Model Oil Preparation

For model oil preparation, which is the representation of crude oil for bigger process, it is prepared by mixing together Dodecane and calculated amount of Dibenzothiophene so that the concentration of DBT in Dodecane is 0.1wt%. (The calculation for amount of dodecane needed is available at Appendix C)

3.3.2   Experimental Materials and Apparatus

Below is the list of chemicals and apparatus needed to conduct the photocatalytic desulfurization analysis experiment:

| Chemicals	Apparatus
Model Oil Prepared	500W medium pressure Hg lamp with pyrex well
Ionic liquid prepared [BMIM]FeCl$_4$	50ml 3 neck round-bottle flask
Photocatalysts prepared: Fe/TiO$_2$	Magnetic Stirrer
	Needle and Syringe
	GC Analyzer

TABLE 3.2: Chemicals and apparatus for the experiment

3.3.2 Desulfurization Procedure using Halogen Lamp

The desulfurization experiment is been carried out to observe the photocatalytic ability of the Fe/TiO$_2$ photocatalysts and extraction process by [BMIM]FeCl$_4$ for sulfur removal in model oil. The experiment is prepared by adding 0.1g 0.4FeTiO400 in 20ml of model oil. The solution is being stirred for 30 minutes (without irradiation of light) to ensure well mixing of photocatalyst in model oil. Then, the mixture is subjected to irradiation with a visible light source after the first 30 minutes. The whole reactions were carried out for 5 hours (including 30 minutes without visible light irradiation). The sample of model oil is being taken after at the initial and final of the experiment. The sample is subjected to centrifugal force to separate the oil phase and photocatalyst. The oil phase of the samples were taken and sent to Gas Chromatograph analysis (GC) to determine the amount of sulfur left in the oil phase. The procedure is repeated for 5 other modified photocatalyst, pure TiO$_2$ and [BMIM] FeCl$_4$. For [BMIM]FeCl$_4$, model oil is added to [BMIM]FeCl$_4$ with a ratio of 20:1 (model oil: ionic liquid) in term of weight. The result is studied and the best Fe/TiO$_2$ photocatalyst is determined.

The experiment followed for integrated approach using photocatalytic desulfurization and ionic liquid extraction. Model oil is added to [BMIM]FeCl$_4$ with a ratio of 20:1 (model oil: ionic liquid) in term of weight. 0.1g of the best Fe/TiO$_2$ photocatalyst is added for every 20ml of model oil. The best photocatalyst is added to solution of model oil and [BMIM]FeCl$_4$ to determine the ability of sulfur removal by photocatalysis and ionic liquid extraction at the same time. The reactions were carried out for 5 hours and samples at the intial and final experiment are taken. The samples are centrifuged to separate the oil phase with the ionic liquid phase. The oil phase of the samples was sent to Gas Chromatograph analysis (GC) to determine the amount of sulfur left in the oil phase. Figure 3.5 is the summary of the desulfurization from model oil experiment.
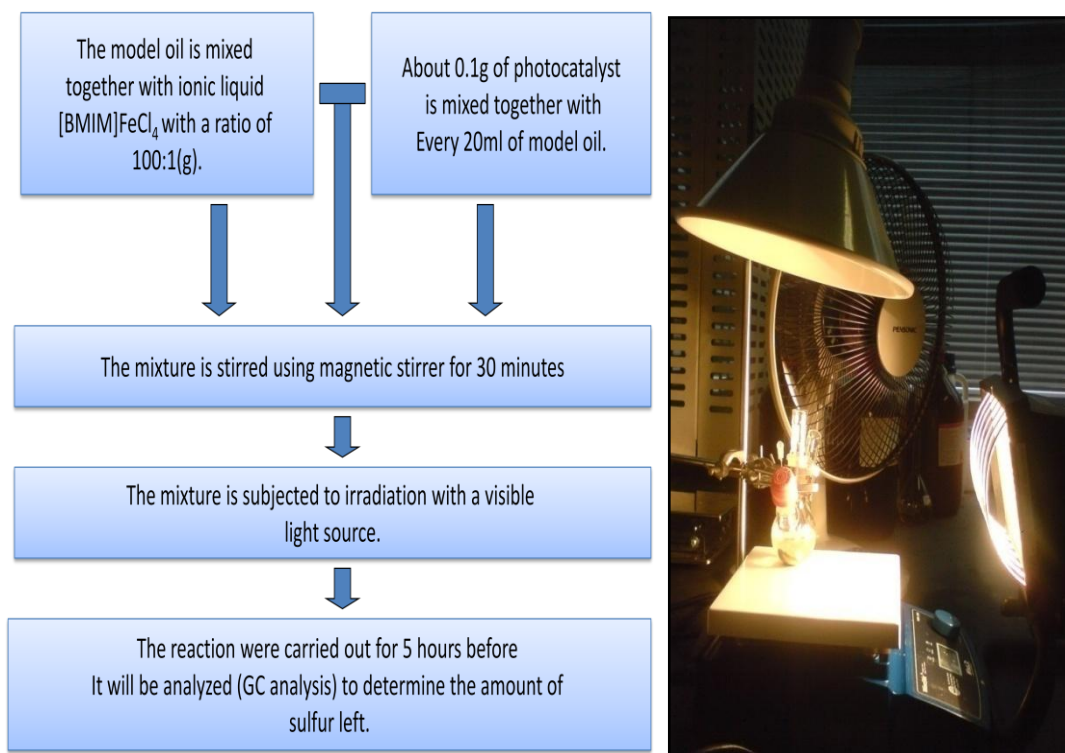
FIGURE 3.5: Experimental Procedure for Photocatalytic Desulfurization Experiment (left) and picture of the setup of the experiment (right)

3.3.3 Amount of Sulfur in Model Oil, [S] Monitoring

After the experiment, the samples are centrifuged to separate the oil phase with the ionic liquid phase. The samples then are analyzed using GC (Gas Chromatography) analysis to determine the amount of sulphur left in model oil. This test is to determine the degree of success for pure TiO_2 and modified TiO_2 to remove sulfur from the model oil. GC Analyzer use the area under the peak of the curve from the sample to calculate the concentration of the remaining sulfur in samples by calibrating it with the curve from standard samples that have been sent earlier.

CHAPTER 4

RESULT AND DISCUSSION

4.1 Characterization of Photocatalysts, Fe/TiO$_2$

To observe and analyze the distribution of dopant element inside TiO$_2$ structures, chemical and physical properties, the modified photocatalysts are characterized using several method of analysis, focusing on elemental analysis to determine the element exist in modified photocataysts, the metal distribution and optical properties to observed the changes of Band gap energy after the modifications are done so that correlations can be done with the observed performance of modified photocatalysts. Below are the result analysis from samples prepared fpr XRD test, UV-vis DRS analysis, FE-SEM analysis and FTIR test.

4.1.1 X-Ray Diffraction (XRD)

All of the photocatalysts prepared were subjected to XRD analysisand the result of the test represent by XRD diffractogram of the samples are shown in Figure 4.2. As for comparison, XRD diffractogram of pure TiO$_2$ is also included and shown in Figure 4.1 below:

FIGURE 4.1: Pure TiO$_2$ XRD Diffractogram

From Figure 4,1, as shown in the pure TiO$_2$ diffractogram, the diffracton peaks at 2θ = 25.34°, 37.9°, 48°, 53.9° and 55° represent indices of (101), (004), (200), (105) and (211) phase plane, in which were confirmed to be crystalline structure of TiO$_2$ anatese. (Yoong L. S., *et al*, (2009)). As shown in Figure 4.2, observing the XRD diffractogram for other modified photocatalysts, all of diffraction patterns from samples showing quite similar pattern and peaks at the same point, showing that all samples exhibit only patterns assigned to the well crystalline anatase phase (Zhu, J., *et al.* (2004)).

For low Fe content, any crystalline phase containing Fe could not be observed by XRD in Fe/TiO$_2$. It is due to the fact that Fe^{3+} and Ti^{4+} have similar ionic radii (0.79Å versus 0.75 Å), so Fe^{3+} can easily substitute Ti^{4+} into TiO$_2$ lattice. These results support that the current doping procedure allows uniform distribution of the dopants, forming stable solid solutions within TiO$_2$. From the diffraction patterns it is also obvious that the materials prepared are in the form of small particles, as the peaks are broad (Zhu, J., *et al.* (2004)). So, Fe$_2$O$_3$ or Fe$_x$TiO$_y$ phase also could not be found in XRD diffractogram pattern (Zhou M, *et al.* (2006)) which meant that Fe$_2$O$_3$ may be existed in amorphous phase (Li Z., *et al*. (2008)).

FIGURE 4.2: Pure TiO_2 and modified Fe/TiO_2 XRD Diffractogram

27

4.1.2   UV-vis Diffuse Reflectance Spectra (DRS)

The DR-UV-Vis spectra of the catalyst samples as well as of pure TiO2 are depicted in Figure 4.3 and 4.4 (zoomed to be between wavelengths of 350 to 550nm). The spectra of pure TiO_2 shows absorption peak at 388nm which is still in UV region (Yoong L. S., *et al*, (2009)). A significant increase in the absorption at wavelengths shorter than 400 nm can be assigned to the intrinsic band gap absorption of TiO_2 (Zhou M, *et al.* (2006)).

When doped with Fe, considerable shift of the peak towards the visible range at around 400–800 nm occurred for all the samples as shown in clearer view at Figure 4.4. The absorption spectra of the Fe/TiO_2 samples show a stronger absorption in the UV–visible light region and an obvious red shift in the band gap transition. Fe-doping obviously affects light absorption characteristics of TiO_2 as shown in Figure 4.4.With increasing Fe-doping concentration; the samples show a stronger absorption in the visible range and a red shift in the band gap transition. The red shift is ascribed to the results of the Fe-doping (Zhou M, *et al.* (2006)). It is also observed that Fe/TiO_2 samples calcined at 500°C have slightly more absorption than those calcined at 400°C with given amount of dopant. Increment of light absorption of the samples in visible light region can possibly lead to better photocatalytic activity, especially under visible light region.
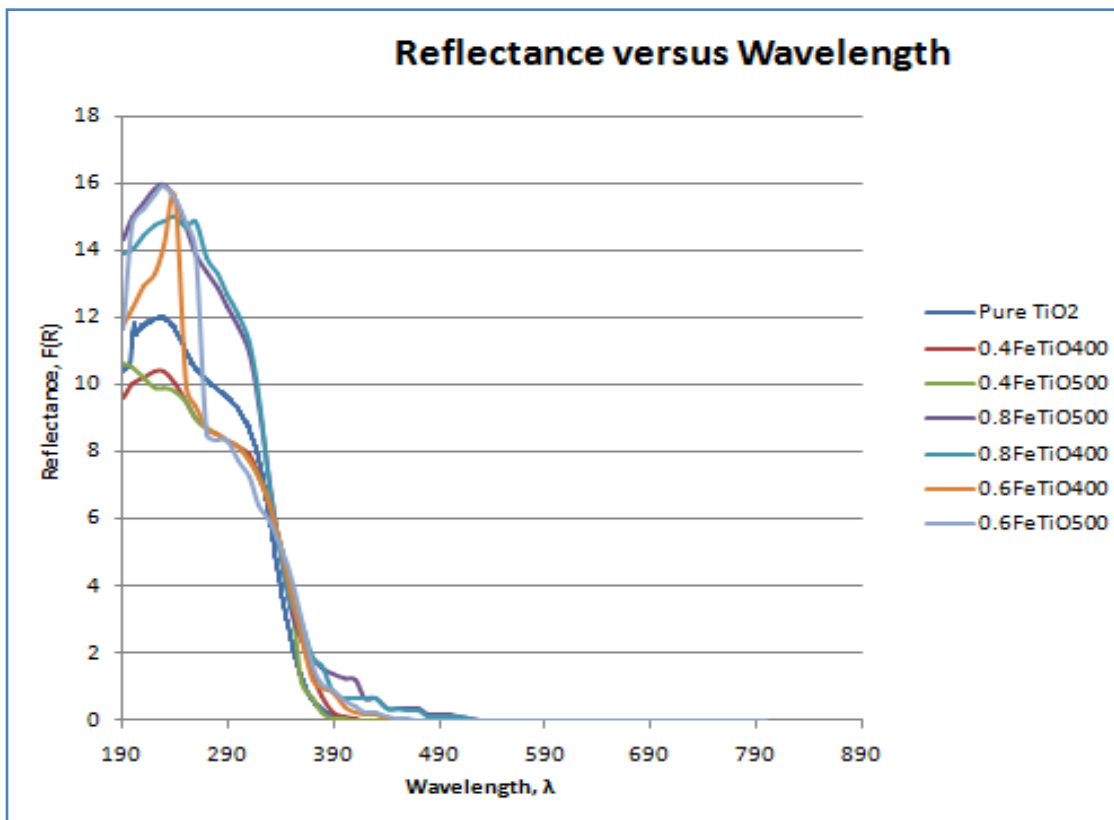
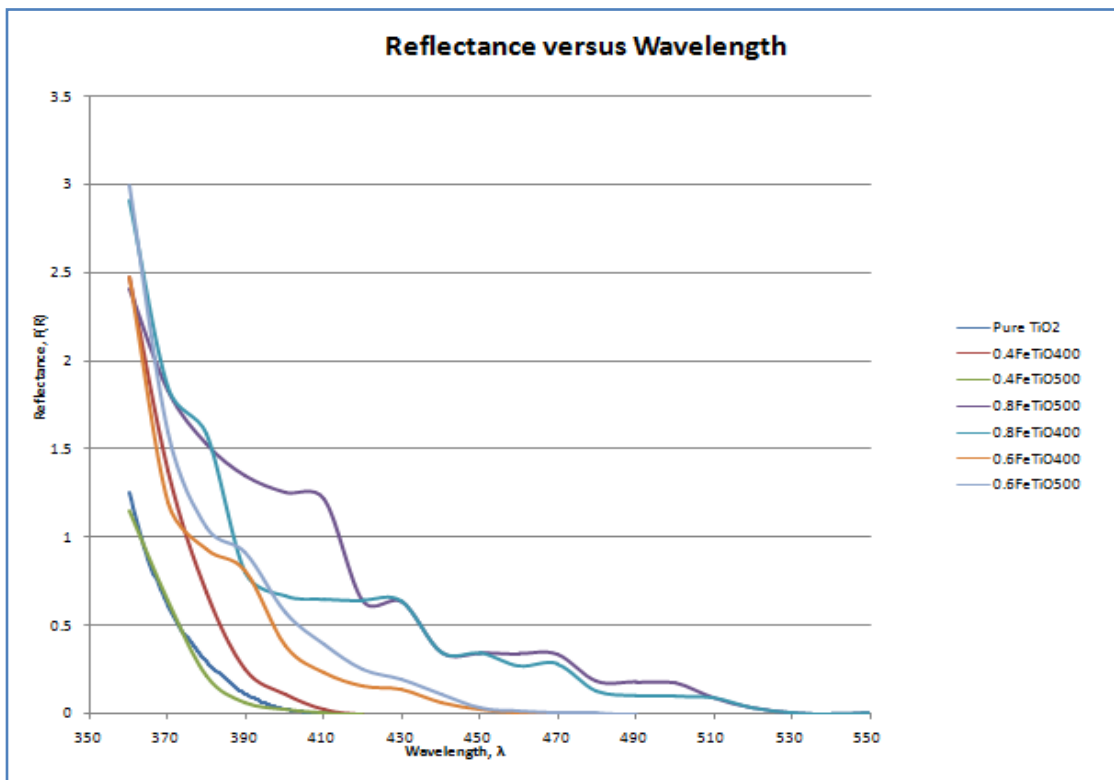**FIGURE 4.3**: DR-UV-vis spectra for pure TiO_2 and Fe/TiO_2 samples

FIGURE 4.4: DR-UV-vis spectra for pure TiO_2 and Fe/TiO_2 samples (350-550nm)

The UV-Vis absorption edge and band gap energies of the samples have been determined from the reflectance [F(R)] spectra using the KM (Kubelka–Munk) formalism and the Tauc plot. For a semiconductor material, a plot of $[F(R).hv]^n$ against hv should show a linear region just above the optical absorption edge for n = ½ if the band gap is a direct transition, or for n = 2 if it is indirect (Yoong L.S., *et al*, (2009)) . Over the linear region of the plots, the relationship can be described as;

$$[F(R).hv]^{1/2} = K(hv - E_g)$$

Where hv = photon energy, Eg = the band gap energy, and K = a constant characteristic of the semiconductor material. From the equation above, it appears that extrapolation of a Tauc plot to the hv axis should yield the semiconductor band gap energy (Yoong L. S., *et al*, (2009)). The extrapolation lines shown in Figure 4.5 have been used to determine the band gaps for the different catalyst samples tested. The calculated band gap energy for pure TiO2 is also found to be 3.25 eV from the extrapolation of the corresponding plot. The calculated values of the band gap energy are given in Table 4.1. All the catalysts displayed reduction in their band gaps compare to TiO_2.
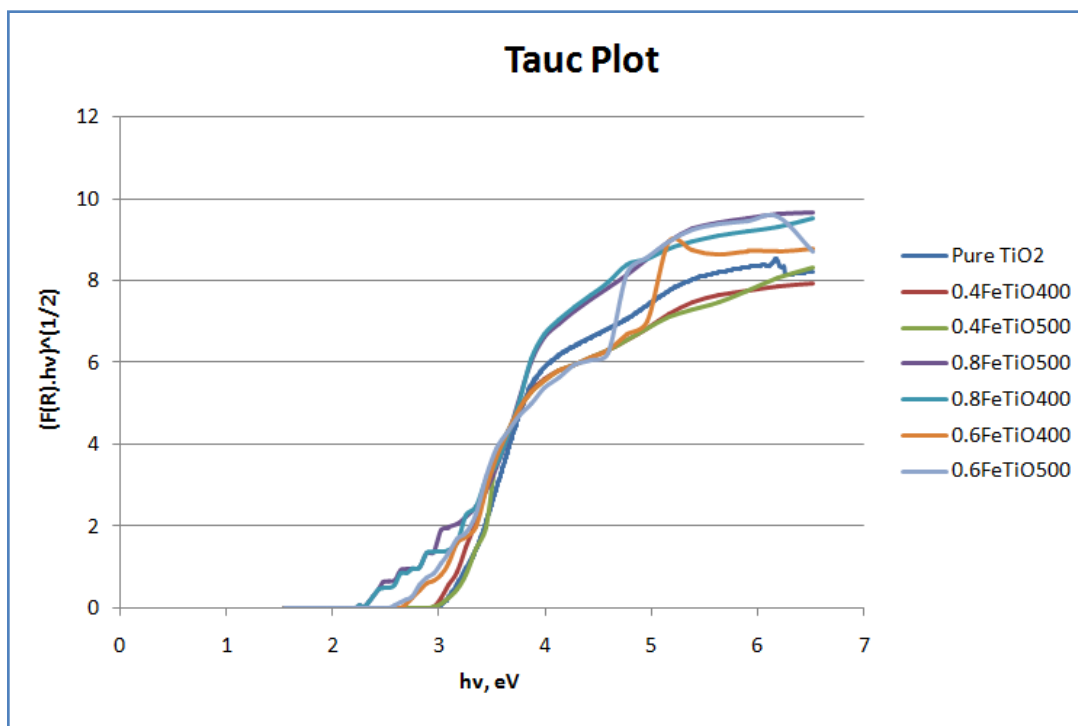
FIGURE 4.5: Plot of transformed Kubelka-Munk function $[(F(R).hv]^{1/2}$ vs hv for pure TiO$_2$ and Fe/TiO$_2$ samples

Reduction of band gap energies of Fe/TiO$_2$ samples increase with the increase of dopant, Fe loading. It is also observed that band gap energies of Fe/TiO$_2$ samples calcined at 500°C is lower than those calcined at 400°C, concluding that higher calcination temperature result in lower band gap energy of the samples. Thus, among the Fe/TiO$_2$ samples, 0.8wt% Fe/TiO$_2$ calcined at 500°C shows the smallest band gap energy at 2.84eV. The summary of the calculated values of band gap energy of all samples is shown in Table 4.1.

| Photocatalyst Samples	Band Gap Energy, eV
Pure TiO_2	3.25
0.4FeTiO400	2.99
0.6FeTiO400	2.96
0.8FeTiO400	2.89
0.4FeTiO500	2.98
0.6FeTiO500	2.90
0.8FeTiO500	2.84

TABLE 4.1: Summary of the Band Gap Energies estimated for UV-vis DRS data

4.1.3 Field Emission Scanning Electron Microscopy (FE-SEM)

All samples of photocatalysts were subjected to FE-SEM scanning, overall consisting 7 samples (Pure TiO_2 and 6 samples of Fe/TiO_2). Figure 4.6 and 4.7 (a)-(f) show the morphology result of the samples from FE-SEM test, showing some irregularities of the samples and variation of particle sizes to be in range of 20-50nm. The irregularities of particle sizes are the result of grinding process on the samples. But, with 100K magnification of scanning is insufficient to observe the distribution of dopant in supported TiO_2 as no real distinction is shown on the morphology results of the modified photocatalysts.
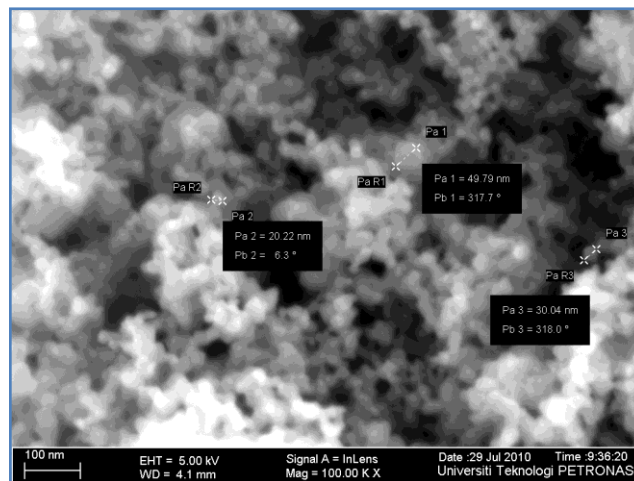
FIGURE 4.6: Morphology result of Pure TiO_2 from FE-SEM
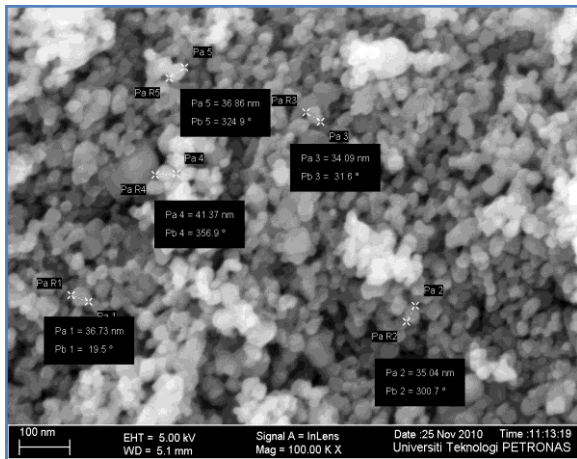
(a) 0.4FeTiO400
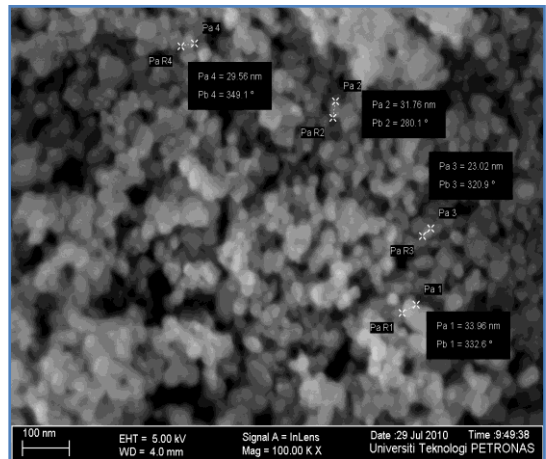
(b) 0.4FeTiO500

(c) 0.6FeTiO400
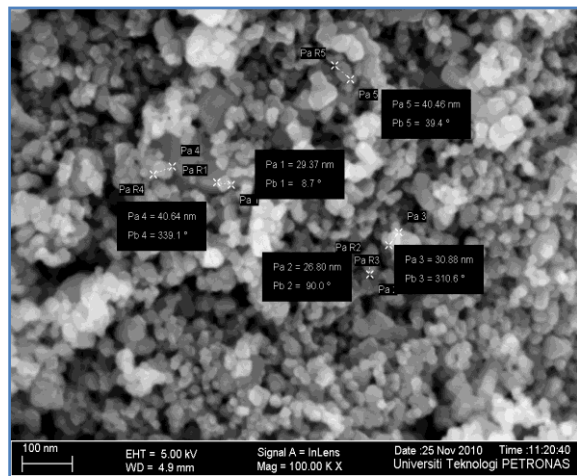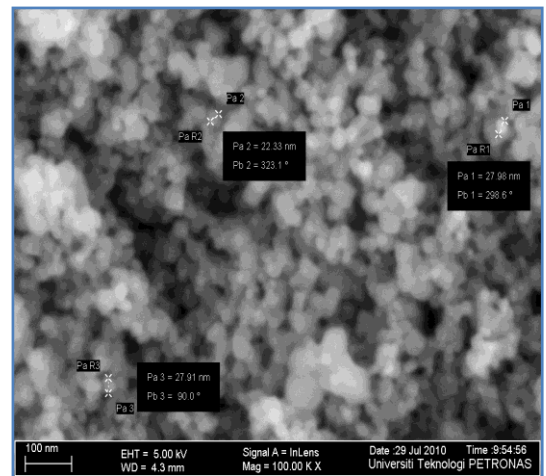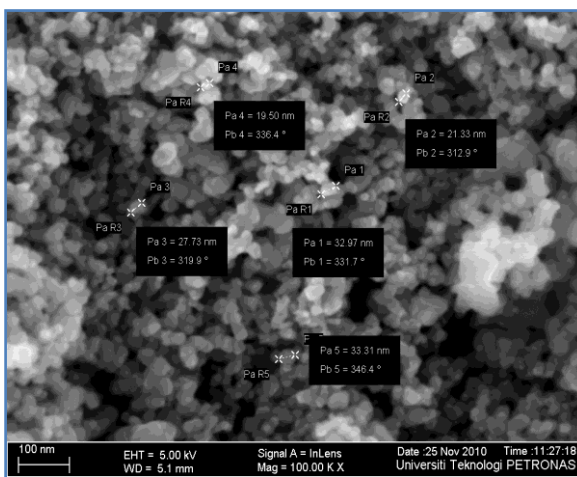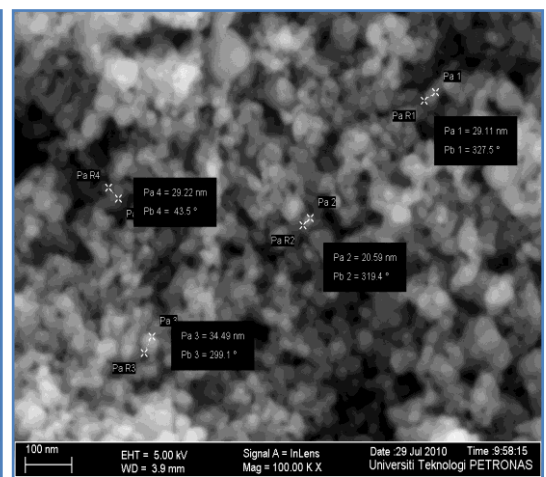
(d) 0.6FeTiO500

(e) 0.8FeTiO400

(f) 0.8FeTiO500

FIGURE 4.7: Fe/TiO$_2$ Morphology Results from FE-SEM

From the morphology results, scanning of 100K magnification is still not sufficient to show the distinction between pure and doped TiO_2, but from elemental analysis using Energy Dispersive X-Ray (EDX) analysis, presence of Fe in prepared photocatalysts can be analyzed. Results from EDX analysis are shown below:
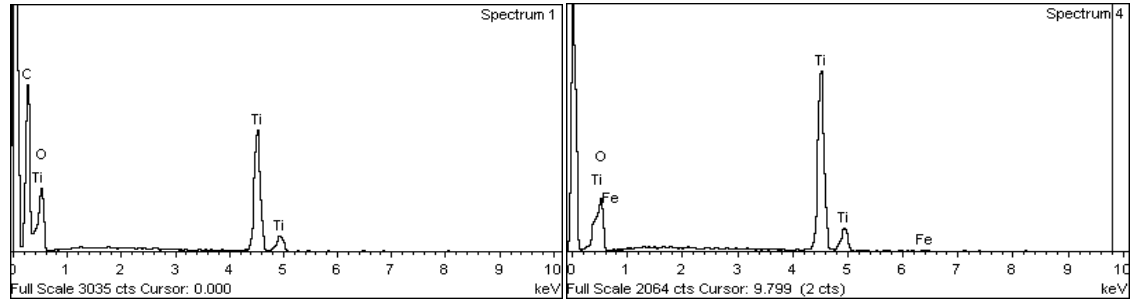
Pure TiO_2 Fe/TiO_2

FIGURE 4.8: Pure TiO_2 and Fe/TiO_2 EDX Results from FE-SEM

As shown in EDX results from Table 4.2 and 4.3 (a)- (f), from elemental analysis, the concentration of Fe metal in TiO_2 are analyzed and the result shows that Fe is presents in Fe/TiO_2 but the values calculated are slightly different than targeted values. This is caused by irregularities of the distribution of Fe in TiO_2. But, as a conclusion, Fe is present in prepared Fe/TiO_2 and well distributed as the error from the targeted value (concentration of dopant) and obtained value exhibit error below than 35%.

Pure TiO_2

Element	Weight%	Atomic%
C K	44.24	57.58
O K	37.22	36.37
Ti K	18.54	6.05
Totals	100.00	

TABLE 4.2: Summary of the EDX Result for pure TiO_2

(a) 0.4Fe/TiO$_2$400

Element	Weight%	Atomic%
O K	40.65	67.22
Ti K	59.07	32.66
Fe K	0.28	0.12
Totals	100.00	

(b) 0.4Fe/TiO$_2$500

Element	Weight%	Atomic%
O K	40.64	67.20
Ti K	59.05	32.61
Fe K	0.31	0.19
Totals	100.00	

(c) 0.6Fe/TiO$_2$400

Element	Weight%	Atomic%
O K	53.04	77.21
Ti K	46.30	22.51
Fe K	0.66	0.27
Totals	100.00	

(d) 0.6Fe/TiO$_2$500

Element	Weight%	Atomic%
C K	5.21	9.03
O K	57.46	74.78
Ti K	36.73	15.96
Fe K	0.61	0.23
Totals	100.00	

(e) 0.8Fe/TiO$_2$400

Element	Weight%	Atomic%
O K	50.32	75.23
Ti K	49.18	24.56
Fe K	0.50	0.21
Totals	100.00	

(f) 0.8Fe/TiO$_2$500

Element	Weight%	Atomic%
O K	50.23	75.09
Ti K	49.08	24.53
Fe K	0.69	0.37
Totals	100.00	

TABLE 4.3: Summary of the EDX Result for Fe/TiO$_2$

4.1.4 Fourier Transform Infrared Spectroscopy (FTIR)

Figure 4.9 shows the FTIR transmission spectra of the Fe/TiO_2 photocatalyst for before calcination. As shown in Figure 4.9, in all the spectra, the absorption peaks around $1600cm^{-1}$ and $3400cm^{-1}$ are attributed to the O–H bending and stretching ,respectively while the IR band observed from 400 to $900cm^{-1}$ corresponds to the Ti–O stretching vibrations. The IR band also shows the absorption band at 1382.7 cm-1 which is attributed to the presence of nitrate (NO_3^-) group in the samples tested (Yoong L. S., *et al*, (2009)). This peak is seen clearly as the samples are yet subjected to calcination process which purposely done to remove nitrate (NO_3^-) group (Yoong L. S., *et al*, (2009)).
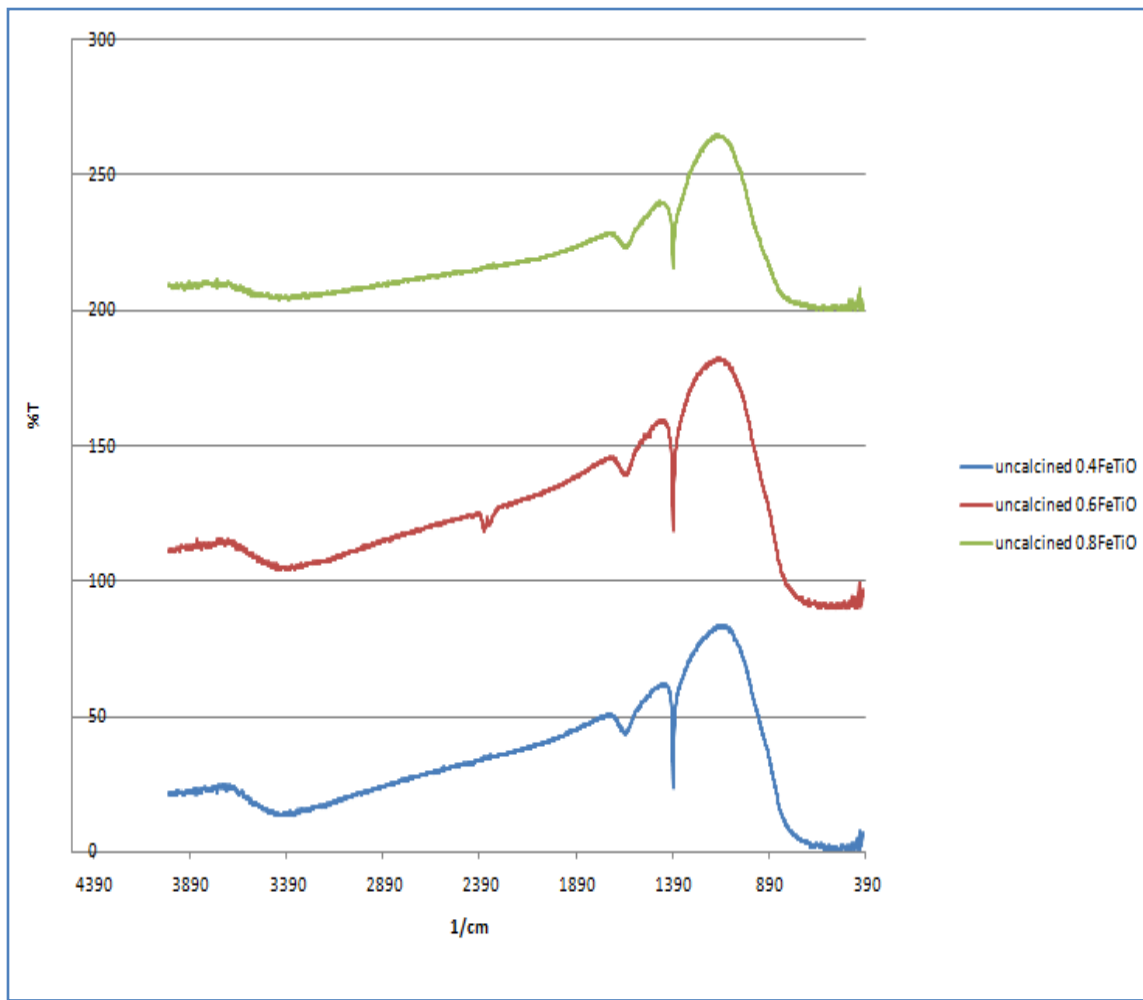
FIGURE 4.9: FTIR spectra for Fe/TiO_2 samples before calcination

36

As for samples after calcinations, the FTIR spectra of the samples are shown in Figure 4.10 below. As observed, the absorption peaks around $1600cm^{-1}$ and $3400cm^{-1}$ and 400 to $900cm^{-1}$ are still detected in calcined samples. On the other hand, the absorption band at 1382.7 cm^{-1} which is attributed to the presence of nitrate (NO_3^-) group could not be detected on the spectra shown in Figure 4.10, spectra for samples after subjected to calcination at $400°C$ and $500°C$, indicating that the calcination process was able to completely remove the NO_3^- group from the raw catalysts.
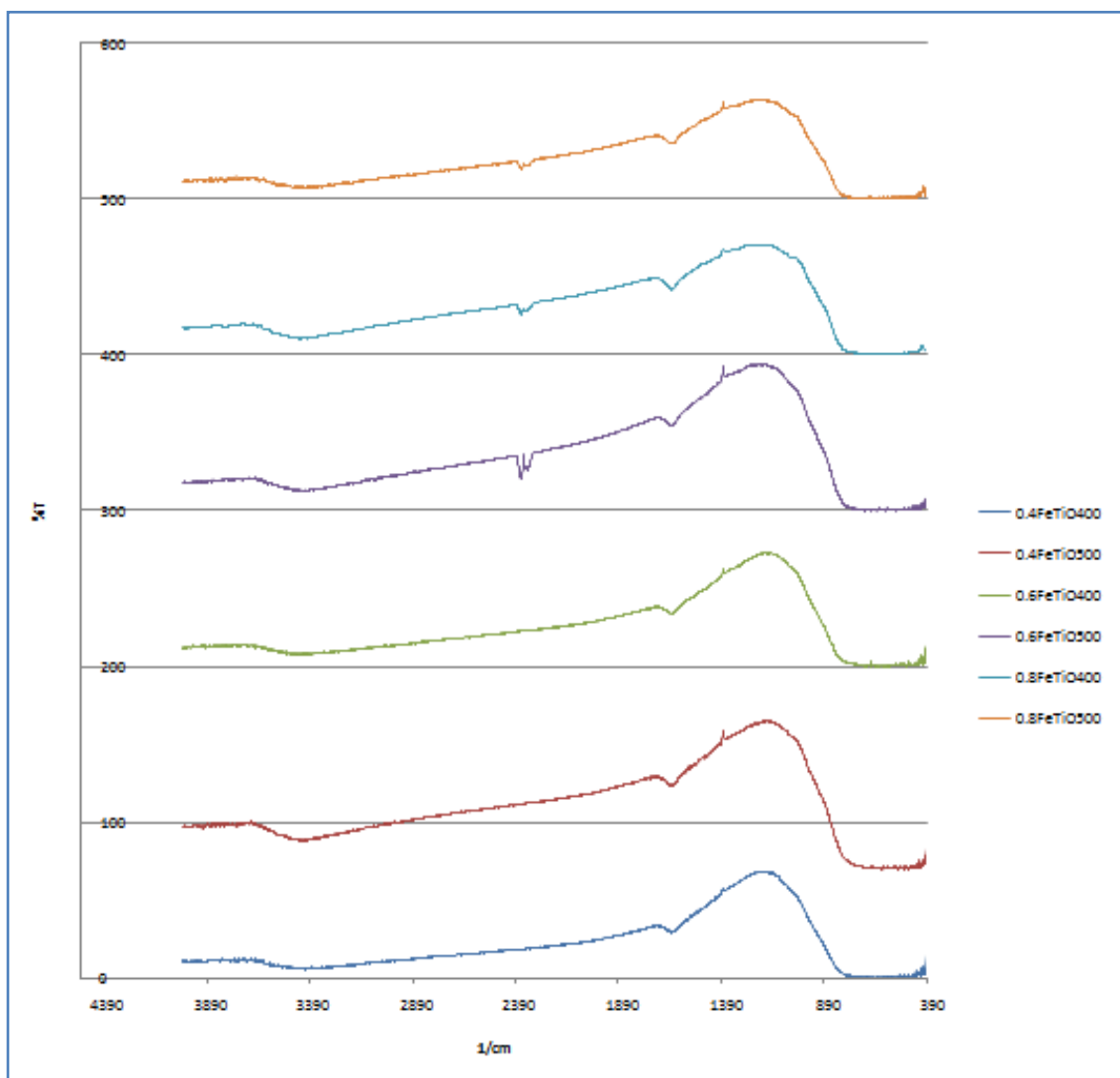
FIGURE 4.10: FTIR spectra for Fe/TiO$_2$ samples after calcinations

4.2 Desulfurization of Model Oil using Fe/TiO$_2$ and [BMIM]FeCl$_4$

Desulfurization process represents the observation on the sample of photocatalysts (pure TiO$_2$ and Fe/TiO$_2$) regarding the improvement of the photocatalytic activity of the modified photocatalysts and the extraction process by the ionic liquid, [BMIM]FeCl$_4$. All 7 samples of photocatalysts were used in desulfurization experiment, plus one ionic liquid, [BMIM]FeCl$_4$, tested one by one before the best among the tested photocatalysts is obtained to be combined with [BMIM]FeCl$_4$ as the integrated approach for desulfurization process.

The results from the desulfurization experiment are shown in Table 4.4. As the methodology specified in previous section, the samples were taken at the initial and final of the experiment. The result of GC analysis of initial amount of Sulfur in model oil is 0.112wt%. As for final concentration of Sulfur in samples, the results are listed in Table 4.4. The results show that the desulfurization process, from the pattern of results, percentage of sulfur removal increases from Fe/TiO$_2$ concentration of 0.4 to 0.6wt% and decrease from 0.6 to 0.8wt%. Besides, the photocatalytic activities of the prepared photocatalysts reduce with the increasing of calcinations temperature.

The results show that the desulfurization process, from the pattern of results, percentage of sulfur removal increases from Fe/TiO$_2$ concentration of 0.4 to 0.6wt% and decrease from 0.6 to 0.8wt%. Besides, the photocatalytic activities of the prepared photocatalysts reduce with the increasing of calcinations temperature.

Samples	Total Sulfur Left (%wt)	Percentage of Sulfur Removal (%)
Initial Amount of Sulfur in model oil from GC analysis = 0.112 wt%		
[BMIM]FeCl$_4$	0.083	25.55
Pure TiO$_2$	0.110	1.79
0.4FeTiO400	0.106	5.36
0.6FeTiO400	0.104	7.14
0.8FeTiO400	0.106	5.36
0.4FeTiO500	0.107	4.46
0.6FeTiO500	0.105	6.25
0.8FeTiO500	0.106	5.36
[BMIM]FeCl$_4$+ 0.6FeTiO400	0.071	36.61

TABLE 4.4: Summary of Sulfur Removal Experiment Result

Doping of Fe^{3+} has been affirmed to be responsible for the reduction of the photo-generated hole–electron recombination rate and introduce much more oxygen vacancies in/on the crystal lattice and surface of TiO_2, while oxygen vacancies favor the adsorption of H_2O and formation of surface hydroxyl group, as well as promote the photocatalytic activity. (Tianzhong T., *et al.* (2008), Jiefang Z., *et al.* (2006))

$TiO_2 + hv \rightarrow e^- + h^+$ (1)

$Fe^{3+} + h^+ \rightarrow Fe4^+$ (2)

$Fe^{3+} + e^- \rightarrow Fe^{2+}$ (3)

$Fe^{2+} + O_2(ads) \rightarrow Fe^{3+} + O_2^-$ (4)

$Fe^{2+} + Ti^{4+} \rightarrow Fe^{3+} + Ti^{3+}$ (5)

$Ti^{3+} + O_2(ads) \rightarrow Ti^{4+} + O_2^-$ (6)

$Fe^{4+} + OH^-(ads) \rightarrow Fe^{3+} + OH\bullet(ads)$ (7)   (Tianzhong T., *et al.* (2008))
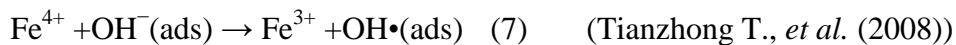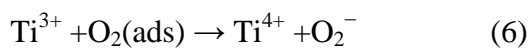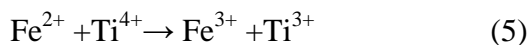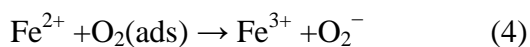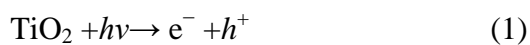
Unfortunately, Fe^{3+} can also act as the recombination centers for the photogenerated electrons and holes (Eqs. (2 and 3) and (8–10)), thus resulting in the decrease of photocatalytic activity. When the dopant concentration is too high, the recombination rate will increase and compete with the redox processes because the distance between trapping sites decreases. (Tianzhong T., *et al.* (2008), Jiefang Z., *et al.* (2006))

$$Fe^{4+} + e^- \rightarrow Fe^{3+} \qquad\qquad (8)$$
$$Fe^{2+} + h^+ \rightarrow Fe^{3+} \qquad\qquad (9)$$
$$Fe^{2+} + OH\bullet \rightarrow Fe^{3+} + OH^- \qquad\qquad (10) \quad (Tianzhong\ T.,\ et\ al.\ (2008))$$
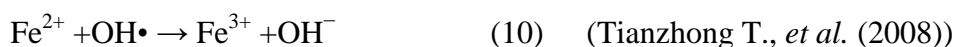
With increasing of calcinations temperature will induce the change in morphologies of the photocatalyst, resulting in reducing of contact area of the particle. Decreasing in contact area for reaction will reduce the reaction itself, thus photocatalytic activities reduces too. But, low calcination temperature will not be sufficient enough to eliminate the functional group which is NO_3^- group that enables the formation of Fe_2O_3 that can affect negatively to the photocatalytic activities.

From the result, Fe/TiO_2 of 0.6wt% Fe calcined at 400°C show the best result, combining with ionic liquid [BMIM]FeCl$_4$ forming integrated sytem enhance the sulfur removal from 7.14% (0.6FeTiO$_2$400 alone) and 25.55% ([BMIM]FeCl$_4$ alone) to 36.61%. Photooxidation by the photocatalyst converts the sulfur species to sulfone and sulfoxide, smaller compounds and highly polarized that ease the extraction using ionic liquid from model oil that is non polar, thus enhancing the sulfur removal. So, combining both photooxidation and extraction yield better desulfurization.

CHAPTER 5

CONCLUSION AND RECOMMENDATION

5.1 Conclusion

The experimental results on desulfurization process for the pure TiO_2, six modified photocatalyts, Fe/TiO_2 prepared with different dopant loadings and under different conditions of calcinations and ionic liquid, $[BMIM]FeCl_4$ show some definite trends. The sulfur removal of Fe/TiO_2 is much higher than that achieved with pure TiO_2 alone. With trend observed, it showed the increment of photocatalytic activity from dopant loading of 0.4wt% to 0.6wt% and decrement when dopant loading increase from 0.6wt% to 0.8wt%. Besides, sulfur removal form samples of Fe/TiO_2 calcined at 400°C are higher than those calcined at 500°C showing that photocatalytic activity of the photocatalyst depends on the amoung of dopant and calcinations temperature. From all seven samples of photocatalysts prepared, (TiO_2 and Fe/TiO_2) Fe/TiO_2 with 0.6wt% of Fe calcined at 400°C exhibit the best sulfur removal percentages at 7.14% sulfur removal, thus selected to be combined with ionic liquid as Integrated System. Combining with ionic liquid also enhance the desulfurization as extraction is added to the system, leading to photooxidation-extraction integrated system. This is shown in results where sulfur removal is increased from 7.14% (photocatalyst) and 25.55% (ionic liquid) to 36.61% (Integrated System). Photooxidation by the photocatalyst converts the sulfur species to sulfone and sulfoxide, smaller compounds and highly polarized that ease the extraction using ionic liquid from model oil that is non polar, thus enhancing the sulfur removal. So, combining both photooxidation and extraction yield better desulfurization. The size range of the particles sizes for the pure TiO_2 and Fe/TiO_2 catalyst varied between 20 and 50 nm. The relatively uniform dispersion of Fe on TiO2 indicated by the EDX results and the full crystallinity confirmed by the XRD analysis are the factors behind its highest catalytic efficiency.

5.1   Recommendation

For future study and improvement, more characterization method should be done for in-depth studies of the properties of photocatalyst using Brunauer Emmett Teller (BET) Specific Surface Area, X-ray Photoelectron Spectroscopy (XPS), Transmission Electron Microscopy (TEM), Thermogravimetric Analysis (TGA), Temperature-Programmed Reduction (TPR) and Atomic absorption spectrometry (AAS). Modification should be done on the method for preparing modified photocatalyts, to optimize the distribution of the dopant in supported TiO_2. Other method can be suggested such as complex precipitation as this method proposed better distribution of dopant in semiconductor. Calcination temperature and duration can be best determined using TGA analysis. By implying this analysis beforehand, we can increase the efficiency of photocatalyst. Another type of metal transition doping also should be studied for the desulfurization process such as Fe, Mn, Ni, Zn, Pt, Ag, and etc. Study of desulfurization process should be done by other sulphur species such as Benzothiophene and instead of using model oil, the reaction should be continued by using the crude oil so that real efficiency of the desulfurization by both photocatalytic desulfurization and extraction can be observed.

REFERENCES

Aboel M. A., Abdel W., Abde1 A. M. (1998), TiO_2-photocatalytic oxidation of selected heterocyclic sulfur compounds, Journal of Photochemistry and Photobiology A: Chemistry 114, 2l3-218.

Amy L. L., Guangquan L., and John T. Y. (1995), Photocatalysis on TiO_n Surfaces: Principles, Mechanisms, and Selected Results, Chem. Rev. 95, 735-758.

Anisimov A. and Tarakanova A. (2009), Oxidative desulfurization of hydrocarbon raw materials. Russian Journal of General Chemistry 79, 1264-1273.

Campos M. J. M., Capel S. M. C., Perez P. P., Fierro J. L. G. (2010), Oxidative Processes of Desulfurization of Liquid Fuels, Journal of Chemical Technology & Biotechnology 85(7), 879–890.

Chongpin H., Biaohuhen, Jie Z., Zhichang L., and Yingxia L. (2004), Desulfurization of Gasoline by Extraction with New Ionic Liquids, Energy & Fuels 18, 1862-1864.

Dishun Z., Ran L. (2008), Photochemical oxidation-Ionic Liquid extraction coupling technique in deep desulfurization of light oil. Energy & Fuel, 1100-1103.

Hiroaki T., Tetsuya N., Shinya S. (2009), Energy-efficient ultra-deep desulfurization of kerosene based on selective photooxidation and adsorption, Fuel 88, 1961–1969.

Iraj M. B., Majid M. , Shahram T., Valiolah M., Arsalan M. (2010), $H_3PW_{12}O_{40}$–[BMIM]FeCl$_4$: A novel and green catalyst-medium system for microwave-promoted selective interconversion of alkoxymethyl ethers into their corresponding nitriles, bromides and iodides, Comptes Rendus Chimie.

Jiefang Z., Feng C., Jinlong Z., Haijun C., Masakazu A. (2006), Fe^{3+}-TiO_2 photocatalysts prepared by combining sol–gel method with hydrothermal treatment and their characterization, Journal of Photochemistry and Photobiology A: Chemistry 180, 196–204.

Josh A. N., Gem D. C., Marta I. L., Gladi N. B. (1996), Synthesis, characterization and photocatalytic properties of iron-doped titania semiconductors prepared from TiO_2, and iron (III) acetylacetonate, Journal of Molecular Catalysis A: Chemical 106, 267-276.

Yoong L.S., Chong F.K., Binay K. D. (2009), Development of copper-doped TiO_2 photocatalyst for hydrogen production under visible light, Energy 34, 1652–1661.

Li Z., Shen W., He W., & Zu X. (2008), Effect of Fe-doped TiO_2 nanoparticle derived from modified hydrothermal process on the photocatalytic degradation performance on methylene blue, Journal Hazardous Materials, 590-594.

Paul J. D. (2002), Transition metal chemistry in ionic liquids, Transition Metal Chemistry 27, 353–358.

Sang H. L., Sung H. H., Chun Y. Y. and Yoon M. K. (2007), Recovery of magnetic ionic liquid, [BMIM]FeCl$_4$using electromagnet , Korean J. Chem. Eng. 24(3), 436-437

Shadpour M. and Elaheh K. (2006), Microwave Heating in Conjunction with Ionic Liquid as a Novel Method for the Fast Synthesis of Optically Active Poly(amide-imide)s Derived from *N,N'*-(4,4'Hexafluoroisopropylidenediphthaloyl)-bis-Lmethionine and Various Aromatic Diamines, Iranian Polymer Journal 15(3), 239-247

Takayuki H., Ken O., and Isao K. (1996), Desulfurization Process for Dibenzothiophenes from Light Oil by Photochemical Reaction and Liquid-Liquid Extraction, Ind. Eng. Chem. Res. 35, 586-589

Tianzhong T., Jinlong Z., Baozhu T., Feng C., Dannong H., and Masakazu A. (2007), Preparation of Ce–TiO$_2$ catalysts by controlled hydrolysis of titanium alkoxide based on esterification reaction and study on its photocatalytic activity, Journal of Colloid and Interface Science 315, 382–388

Tianzhong T., Jinlong Z., Baozhu T., Feng C., Dannong H. (2008), Preparation of Fe^{3+}-doped TiO$_2$ catalysts by controlled hydrolysis of titanium alkoxide and study on their photocatalytic activity for methyl orange degradation, Journal of Hazardous Materials 155, 572–579.

Zhou M, Yu J, Cheng B. (2006), Effects of Fe-doping on the photocatalytic activity of mesoporous TiO$_2$ powders prepared by an ultrasonic method, Journal of Hazardous Materials B137, 1838–1847.

Zhu, J., Zheng, W., He B., Zhang J. & Anpo M. (2004), Characterization of Fe/TiO$_2$ photocatalyst synthesized by hydrothermal method and their photocatalytic reactivity for photodegradation of XRG dye diluted in water, *Journal of Molecular Catalysis A: Chemical 216*, 35-43.

Zolta´n A., Na´ndor B., Tu¨nde A., Gyula W., Pa´l S., Andra´s D., and Ka´roly M. (2008), Synthesis, structure and photocatalytic properties of Fe (III)-doped TiO$_2$ prepared from TiCl$_3$, Applied Catalysis B: Environmental 81, 27–37.

APPENDICES

APPENDIX A: Calculation Fe/TiO$_2$ Preparation

Mass Balance Calculation for Fe Metal Doping

Molecular weight for the chemical used in Fe/TiO$_2$ photocatalyst

- Iron(III) Nitrate, Fe(NO$_3$)$_3$.9H$_2$O :   404 g/mol

- Iron metal :   55.85 g/mol

- Titanium Dioxide, TiO$_2$:   79.87 g/mol

Sample calculation (for 0.4 wt% Fe metal doping):

100 g of Fe/TiO$_2$ photocatalyst   →   0.4 g Fe metal needed

20 g of Fe/TiO$_2$ photocatalyst   →   0.08 g Fe metal needed

1 mole of Fe(NO$_3$)$_3$.9H$_2$O   →   55.85 g Fe metal

Therefore, 0.08 g of Fe metal,

$$0.08 \; g \; of \; Fe \; metal = \frac{0.08}{55.85} \times 1 \; mol$$

$$0.08 \; g \; of \; Fe \; metal = 0.001432 \; mol$$

1 mol of Fe(NO$_3$)$_3$.9H$_2$O   →   404 g/mol

Therefore, 0.001432 mol of Fe(NO$_3$)$_3$.9H$_2$O,

$$x \; g \; of \; Iron(III)Nitrate = 404 \; g/mol \; \times 0.001432 \; mol$$

$$0.001432 \; mol \; of \; Iron(III)Nitrate = 0.5787 \; g \; of \; Iron(III)Nitrate$$

Description	Fe^{3+} loading (wt%)		
	0.4	0.6	0.8
Amount of catalyst (g)	20	20	20
Mass of Fe (g)	0.08	0.12	0.16
Mass of TiO$_2$ (g)	19.92	19.88	19.84
Mass of Fe(NO$_3$)$_3$.9H$_2$O (g)	0.5787	0.8680	1.1574

TABLE 7.1: Summary of Fe(NO$_3$)$_3$.9H$_2$O mass needed for respective loading

APPENDIX B: Calculation in Ionic Liquid, [BMIM]FeCl$_4$ Preparation

Molecular weight:

- [BMIM]Cl   = 174.67 g/mol
- FeCl$_3$ anhydrous   = 162.22 g/mol

From the methodology of Ionic Liquid Preparation, equimolar amount of both [BMIM]Cl and anhydrous FeCl$_3$ are needed. So, in preparing 0.5 mole of [BMIM]FeCl$_4$, 0.5 mole of each [BMIM]Cl and FeCl$_3$ are needed. The Calculation for the right amount of reactants to be mixed is as below:

1 mole of [BMIM]Cl → 174.67 g of [BMIM]Cl
So, 0.5 mole [BMIM]Cl = 87.335 g of [BMIM]Cl

As for anhydrous FeCl$_3$
1 mole of anhydrous FeCl$_3$ → 162.22 g of anhydrous FeCl$_3$
So, 0.5 mole anhydrous FeCl$_3$ = 81.11 g of anhydrous FeCl$_3$

So, 87.335 g of [BMIM]Cl is mixed with 81.11 g of anhydrous FeCl$_3$.

APPENDIX C: Calculation in Model Oil Preparation

Dodecane + Dibenzothiophene (0.1wt %)

0.1 wt%　　　→　　　1000ppm　　　→　　　1000 mg/L S

$1 \, L = 1000 \, mg \, S$

$100 \, mL = 100 \, mg \, S$

$1 \, mol \, S = 32.06 \, g \, S$

$1 \, mol \, DBT = 32.06 g \, S$

$1 \, mol \, DBT = 32060 \, mg \, S$

$x \, mol \, DBT = 100 \, mg \, S$

$$x \, mol \, DBT = \frac{100 \, mg \, S}{32060 \, mg/mol \, S}$$

$x \, = 0.003119 \, mol \, DBT$

$$0.003119 \, mol \, DBT = \frac{mass}{184.26 \, g/mol \, DBT}$$
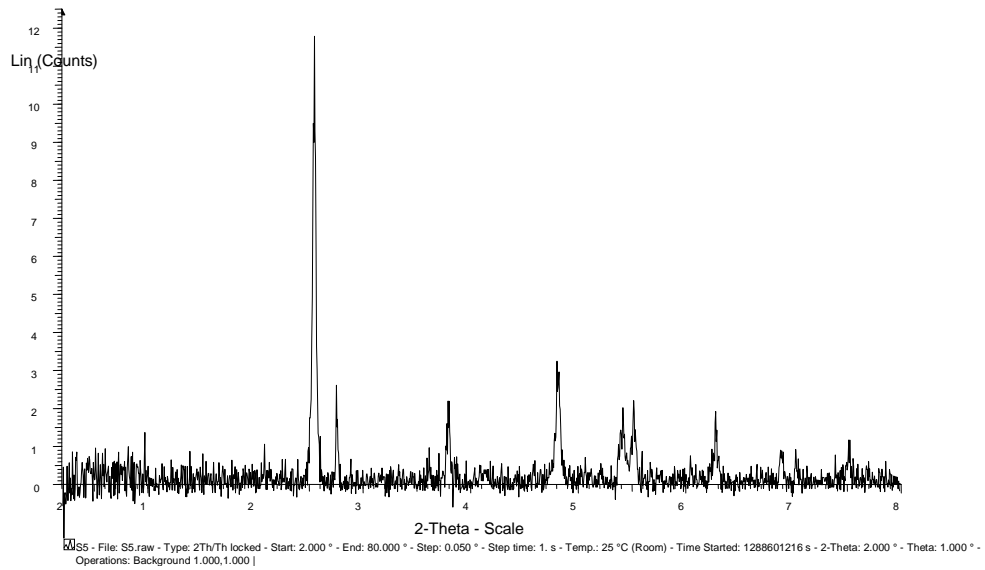
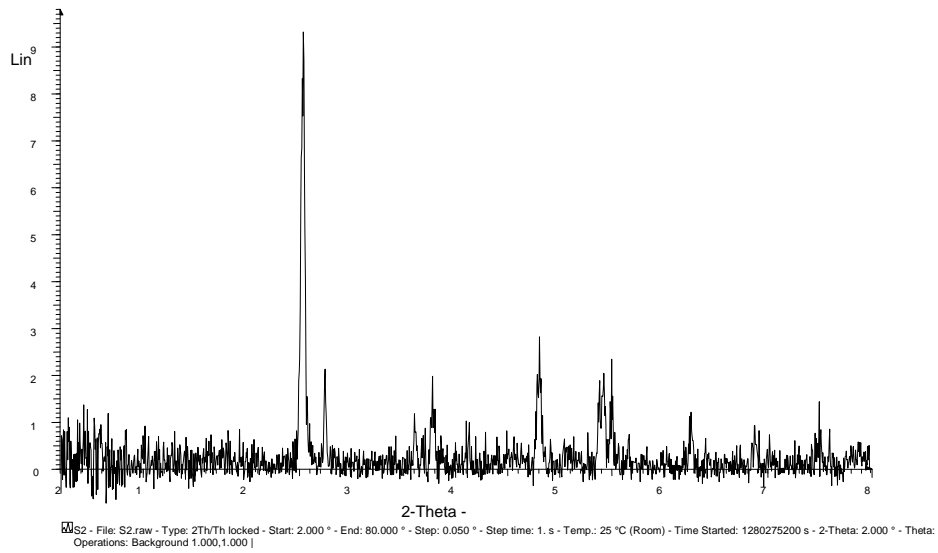$mass = 0.5747 \, g \, DBT$

$y(purity) = 99\%$
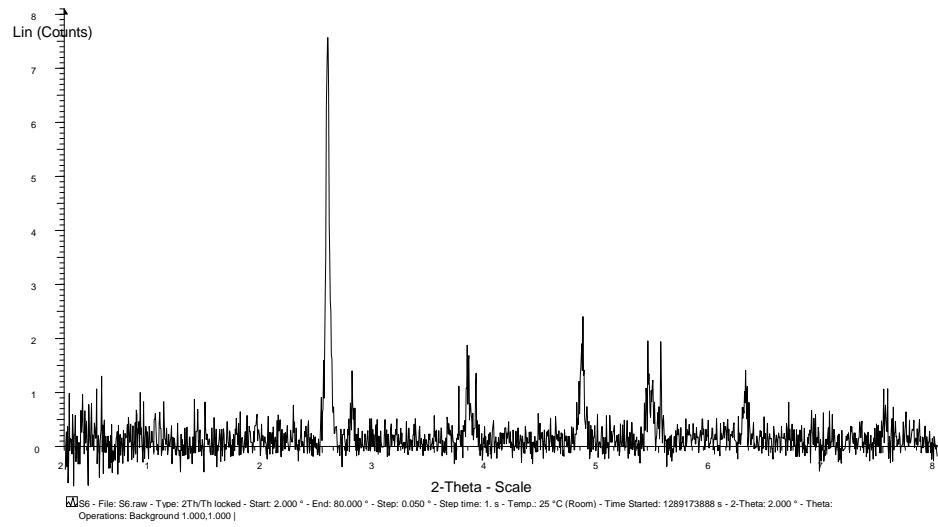
$mass = 0.5747 \div 0.99$

$mass = 0.5805 \, g \, DBT$

APPENDIX D: Result of XRD test for each modified photocatalyst, Fe/TiO₂
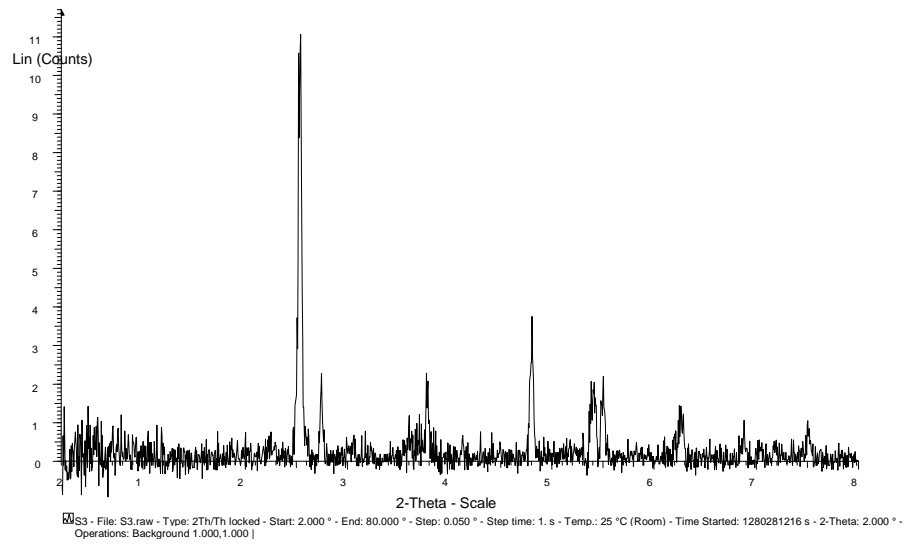

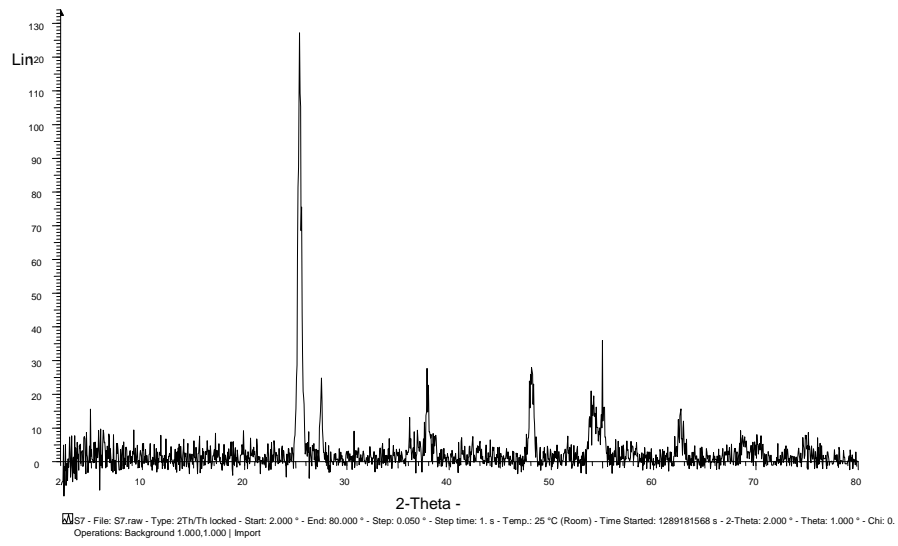FIGURE 8.1: 0.4wt% Fe/TiO₂ calcined at 400°C XRD Diffractogram

FIGURE 8.2: 0.4wt% Fe/TiO₂ calcined at 500°C XRD Diffractogram

Lin (Counts)

2-Theta - Scale

S6 - File: S6.raw - Type: 2Th/Th locked - Start: 2.000 ° - End: 80.000 ° - Step: 0.050 ° - Step time: 1. s - Temp.: 25 °C (Room) - Time Started: 1289173888 s - 2-Theta: 2.000 ° - Theta:
Operations: Background 1.000,1.000 |

FIGURE 8.3: 0.6wt% Fe/TiO₂ calcined at 400°C XRD Diffractogram

Lin (Counts)

2-Theta - Scale

S3 - File: S3.raw - Type: 2Th/Th locked - Start: 2.000 ° - End: 80.000 ° - Step: 0.050 ° - Step time: 1. s - Temp.: 25 °C (Room) - Time Started: 1280281216 s - 2-Theta: 2.000 ° -
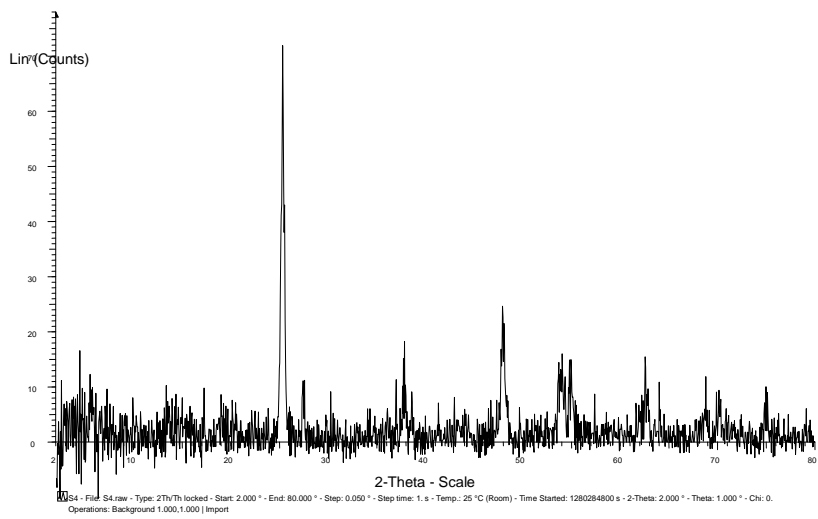Operations: Background 1.000,1.000 |

FIGURE 8.4: 0.6wt% Fe/TiO₂ calcined at 500°C XRD Diffractogram

FIGURE 8.5: 0.8wt% Fe/TiO$_2$ calcined at 400°C XRD Diffractogram

FIGURE 8.6: 0.8wt% Fe/TiO$_2$ calcined at 500°C XRD Diffractogram

APPENDIX E: Result of FTIR test for each modified photocatalyst, Fe/TiO$_2$

1. 0.4wt% Fe/TiO$_2$ before calcination
2. 0.6wt% Fe/TiO$_2$ before calcination
3. 0.8wt% Fe/TiO$_2$ before calcination
4. 0.4wt% Fe/TiO$_2$ calcination at 400°C
5. 0.6wt% Fe/TiO$_2$ calcination at 400°C
6. 0.8wt% Fe/TiO$_2$ calcination at 400°C
7. 0.4wt% Fe/TiO$_2$ calcination at 500°C
8. 0.6wt% Fe/TiO$_2$ calcination at 500°C
9. 0.8wt% Fe/TiO$_2$ calcination at 500°C